QATAR UNIVERSITY

COLLEGE OF ARTS AND SCIENCES

PROPERTIES AND THERMAL STABILIZATION OF NANOCRYSTALLINE COPPER VIA SOLUTE ADDITIONS OF NIOBIUM

BY

MOHAMED A. ABAZA

A Thesis Submitted to the Faculty

of the College of Arts and Sciences

in Partial Fulfillment

of the Requirements

for the Degree of

Masters of Science in

Material Science and Technology

June 2017

COMMITTEE PAGE

The members of the Committee approve the Thesis of Mohamed Abaza

defended on 25/05/2017.

Dr. Khaled Youssef
Thesis/Dissertation Supervisor

Dr. Khalid Al-Saad
Committee Member

Dr. Ahmed Abdalla
Committee Member

Approved:

Rashid Al-Kuwari, Dean, College of College of Arts and Sciences

ABSTRACT

ABAZA, MOHAMED, A., Masters : June : [2017:], Material Science and Technology

Title: Properties and Thermal Stabilization of Nanocrystalline Copper via Solute Additions of Niobium

Supervisor of Thesis: Khaled, M, Youssef.

Nanocrystalline materials, those with grain size <100 nm, were found to have superior mechanical properties compared to their coarse-grained (CG) counterparts. However, these materials are not thermally stable because of having a high density of grain boundaries which increases their Gibbs free energy. Consequently, the nano-grains grow back to their original size in order to release this energy, which results in losing their exceptional properties. Hence, finding ways to stabilize these nano-grains is an utmost importance. Introducing solute to such systems was found to solve the instability issue. Two approaches can describe the mechanism in which the solute atoms prevent or minimize the grain growth, Kinetic Approach which is concerned with reducing the mobility of the grain boundaries by pinning them; and Thermodynamic Approach that works on reducing the energy of the system, hence eliminating the need for the grains to grow.

Nanocrystalline (nc) Cu and Cu-1 at.% Nb are prepared via mechanical ball milling under argon. The microstructure and the properties of the as-milled and the annealed samples are characterized using XRD, TEM, Vickers Microhardness, Tensile tests, SEM, and Four-Point Probe technique. Only one atomic percent of Nb is found to enough to thermally stabilize the nanostructure of copper up to 1073 K, which represents 80% of its melting point. Solute drag and Zener pinning are found to be the main kinetic stabilization mechanisms that succeeded to keep the grain size in the

nanoscale. In addition, the solute atoms substantially enhanced the strength and hardness of the nc Cu, along with maintaining a better ductility. Moreover, such small amount of Nb did not sacrifice the excellent electrical conductivity of copper. This approach of synthesizing and improving the thermal stability of nc materials is not necessarily limited to Cu and could be applied to other metals and alloys. This shall make a leap forward in the production of thermally-stable and ultra-tough nanocrystalline materials for many industrial applications, without affecting their inherent properties.

DEDICATION

This thesis is dedicated to my family, who are the main responsible for my success through their continuous reassurance and support.

ACKNOWLEDGMENTS

A two-year journey would not have been that fruitful without the help of some persons whom I owe them a debt of gratitude.

Firstly, I would like to convey my sincere thanks, appreciation, and gratitude to my supervisor, Dr. Khaled Youssef, for the kind guidance and assistance he gave to me over the two years, and for helping me taking my first steps in the research career. I have learned a lot from him not only on the scientific side but the on the practical side as well. His professional way in working and dealing with obstacles have radically reshaped my personality in a better way.

I also would like to thank my committee members; Dr. Khalid Al-Saad and Dr. Ahmed Abdalla, for their precious time and advice that have significantly contributed to the strength of this thesis.

My acknowledgment also extends to the faculty members; Dr. Ahmed Elzatahry, Dr. Aboubakr Abdullah and Dr. Talal Altahtamouni, whom have added valuable knowledge and skills to me through teaching me the courses of the Master program, which have enriched my background with the fundamentals of the Materials Science, and made it easier for me to go through this research.

Special thanks to Dr. Nasser Alnuaimi, the director of the Center for Advanced Materials, for giving me the opportunity to use the CAM facilities.

Finally, I'd like to express my great appreciation to Prof. Mariam Al-Maadeed, the VP of research and graduate studies at Qatar University, for accepting me as a Master student in the Materials Science and Technology program and as Graduate Assistant, and for her encouragement to maintain an exceptional academic record.

TABLE OF CONTENTS

LIST OF FIGURES

CHAPTER 1: INTRODUCTION

Over the centuries, materials scientists and metallurgists have been doing research to enhance the materials' strength and hardness in order to achieve better performance, especially in high-temperature environments. The advancements in nanotechnology and high-tech industries have added to these efforts. Production of materials with nano-grains (grain size <100 nm) has been found to greatly enhance their strength and the hardness [1]–[8], which may reach to an order of magnitude higher than their conventional CG counterparts [1]. However, it severely reduces their ductility [5], [9]. The reason behind such mechanical performance lies in the grain refinement. This is mainly because more refinement to the grains is escorted by the formation of more grain boundaries, which acts as a barrier to dislocation motion [5]. Further explanation of the relation between grain size and grain boundaries is provided in section 2.1, and their influence on the mechanical properties is addressed in section 2.2.

There are various techniques to synthesize such nanocrystalline (nc) materials, which are all belonging to either of two main synthesis approaches, i.e.; top-down and bottom-up. However, it has been found that each method produces different nanostructure, which in turns results in having different properties even for the same exact produced material of same chemical composition [10]. Hence, choosing the suitable method is important to achieve desirable results. Different production techniques are mentioned in section 2.3, highlighting the energy ball milling technique, as a subcategory of severe plastic deformation, which belongs to the Top-down approach.

Copper is the best electrical and thermal conductive metal after the more expensive silver [11], [12]. This made the world agree to consider copper as a standard

material for measuring the electrical conductivity, known as “International Annealed Copper Standard” (IACS). That is why copper is excellent candidate for many applications which serve plenty of fields, such as wires and cables [13], electric motors [14], heat sinks for electronic devices [15], heat exchanger for pipelines systems, cars’ radiator coils, and air conditionings [16].

Most of the copper uses are in the form of a pure metal. However, it is alloyed when a higher hardness is needed, which represents about 5% of the total use [17]. Unsurprisingly, alloying significantly reduces the excellent properties of the ultra-high electrical and thermal conductivities. Hence, it is of a great interest to achieve higher mechanical properties of copper without sacrificing its inherent properties. Producing it in nc form should help achieving this target. However, nc materials, in general, suffers from thermal instability issues, due to the higher energy that accompanies the high density of grain boundaries. This means that nc materials are prone to grain growth back to their conventional grain size with increasing temperature, hence they lose the unique strength and hardness, which are advantages of nc materials [18], [19]. More details on the instability issue are discussed in section 2.4.

Previous research efforts have concluded that nc alloys and nc materials containing impurities attain substantial thermal stabilization [20]–[27], meanwhile pure nc materials do not. Consequently, it is understood that the solute atoms play a vital role in achieving thermal stabilization in this class of materials. There are two different scenarios describing such role. In the first scenario, the solute atoms kinetically stabilize the grains by pinning them in place, hence preventing their growth. Meanwhile, in the second scenario, the solute atoms reduces the overall energy of the system, hence stabilizing it in a thermodynamic way [28]. More details on the stabilization

mechanisms, as well as some relevant examples from the literature on the thermal stability in nc materials, in general, and nc copper, in particular, are provided in section 2.4.

In this thesis, nc Cu and Cu-1 at.% Nb are prepared via ball milling under argon and characterized using various techniques in order to know their properties. Further details on the preparation methods and the used tools for characterization are provided in Chapter 3. Nb was chosen to thermally stabilize the nanostructure of nc Cu, thanks to the large atomic size misfit, and the positive heat of mixing (ΔH_{mix} = 3 KJ/mol [29]) of the two elements. This shall promote the segregation of Nb atoms to thermally stabilize the system. Adding only 1 at.% Nb has thermally stabilized the grain size of nc Cu up to 80% of the melting point and retained remarkable high strength, ductility, strain hardening, and electrical conductivity as found in chapter 4.

1.1 Novelty and Significance

There are very limited research groups who have worked on nc Cu-Nb system. Yet, all of them were concerned with studying nc Cu alloys with Nb content varying from 5 to 20 wt.% (~3.5 - 14.5 at.%), which is found in the work of Abad et al. [30], Botcharova et al. [31]–[34], and Lei et al. [35]–[38]. Such additions of high-atomic percentage of Nb in Cu causes significant deterioration in its properties. For example, the electrical conductivity of ball milled nc Cu-10%Nb was only about 10% IACS [34]. Mula at al. [39] prepared nc Cu-(1-10 at.%) Nb and examined their properties using XRD and microhardness tests without further investigations, e.g. using TEM and tensile testing. The key to achieve strong and thermally stable nanostructure while preserving other good properties is to minimize the amount of solute additions. The

uniqueness of this thesis arise from being the first to report TEM and HRTEM micrographs, electrical resistivity, and tensile test results of nc Cu-1 at.% Nb. This very small addition of solute Nb helps to maintain the high thermal and electrical conductivities of the pure copper, along with enhancing the strength and hardness of the nanocrystalline copper to more than 10 times those of the conventional pure one. Moreover, the production processes and the stabilization approaches used in this thesis could be applicable to other metals/alloys to enhance their mechanical properties while preserving their own characteristic properties, which widen their utilization in many technological applications.

1.2 Objective and Hypothesis

The purpose of this thesis is to thermally stabilize nc Cu with the addition of 1 at.% Nb and investigate its properties and the stabilization mechanisms.

The hypothesis of the thesis is: Adding only 1 at.% Nb to nc Cu is enough to thermally stabilize its nanostructure and prevent grain growth by reducing the mobility and the free energy of the grain boundaries.

CHAPTER 2: LITERATURE REVIEW

2.1 Nanocrystalline Materials

A nanocrystalline (nc) material is any solid (single/multiphase) with grain size <100 nm [3], [19], [35]. Such material exhibits different physical, mechanical, thermal, optical, and magnetic properties when compared to their conventional CG counterpart (this with grain size >1 μm) [25], [40]–[45]. Nanocrystalline materials can be classified into three main classes relative to their dimensionalities. These classes are one-dimensional (1D) layered structure, two-dimensional (2D) filamentary or rod-like structure, and three-dimensional (3D) equiaxed nanostructure [19],[40]. In this thesis, we are dealing only with bulk nc materials that are made of the consolidation of the 3D equiaxed nanostructured metals. For each of these classes, there are some typical synthesis methods that will be touched upon in section 2.3.

The structure of nc materials consists of nano-grains separated by grain boundaries (GBs). As a result, there are more grains in nc materials compared to their conventional counterpart, hence they have higher volume fraction of GB. Therefore, the number of the interfacial atoms (those lies in the GB regions) is larger than that of the CG ones. Such interfacial component represents around 50% of the whole crystal volume at a grain size of 5 nm, and decreases to 30% at a grain size of 10 nm, whereas this percentage is neglected for the CG materials [19]. It should be also noted that these interfacial atoms are highly disordered. Fig. 2.1 shows a model of equiaxed nc-metal. The black circles in this model represent the crystalline region (regions with long-range order), and the white circles represent the interfacial region (disordered intercrystalline region) [46]. Transmission Electron Microscopy (TEM) micrographs for nc Cu (Fig. 2.2) provides an evidence to the concept of the lack of crystallinity at the GB [2].

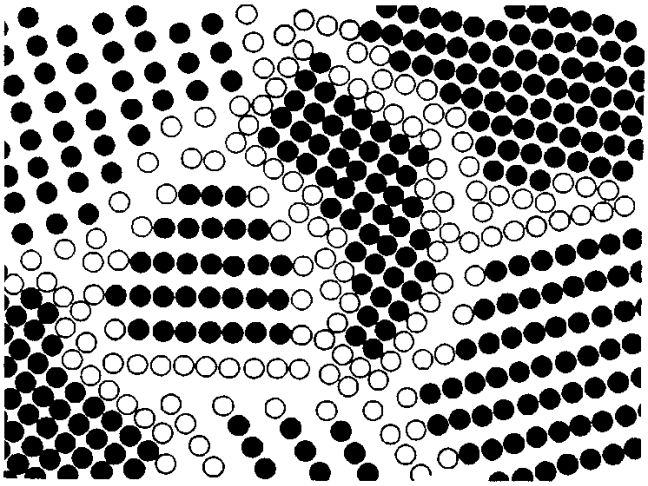

Figure 2.1 Representation of the microstructure for the nc-materials, black circles are atoms belongs to the ordered crystallite regions, and white ones are atoms in the GB regions (interfacial atoms) [46].

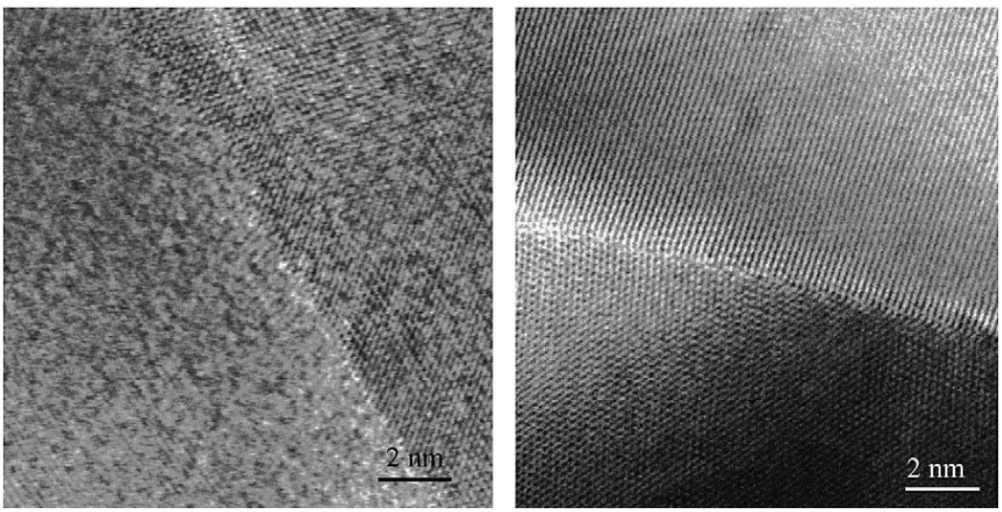

Figure 2.2 TEM images for nc Cu, crystallinity continues up to the GB [2].

2.2 Mechanical Properties of Nanocrystalline Materials

The unconventional structure of the nc materials, previously mentioned, is the main reason why these materials attain superior mechanical properties [47]. Nanocrystalline materials possess ultra-high yield strength that may reach up to 11 times higher than their CG counterparts [3], and this is basically what makes scientists interested in these materials. Grain refinement is considered to be the main tailoring

tool that controls the mechanical properties. However, it has been experimentally proven that different techniques used to produce nc material result in having products with different mechanical properties, even if they have the same grain size and chemical composition. This was attributed to the different flaws and impurities, variations of the dislocation density, and different interfacial structure that each technique may introduce to the final product [8],[48].

The yield strength of the nc metals follows the Hall-Petch relationship in terms of the increased strength with the reduction of crystal size [47]. As per the early predictions made by Gleiter, strength, hardness and ductility of an nc material ought to increase with grain size refinement. Even though most of the experimental work has proved this for the strength and the hardness, but it failed to prove it for the ductility level [4], as can be spotted in the early trial of J.R.Weertman [45]. However, pronounced achievements in maintaining good ductility of nc/nanostructured materials have been reported [3], [6]–[8], [49]–[53].

2.2.1 Strength, Hardness, and Ductility

Several mechanical tests such as hardness [7], [38], tensile [10], [21], [26], [27], compression [34] [56], miniaturized disk bend test (MDBT) [57] have been used to investigate the mechanical properties of nc metals and alloys. Legros, et al. [45] produced nano-grained Cu via inert gas condensation using resistive heating to evaporate pure Cu, then they warm compacted the sample at 150 °C (0.31 T_m) for 4 hr. The micro-sample tensile test done for this sample showed higher yield stress (0.2% offset) of 535 MPa compared to the 340 MPa of the sample produced by Wang et al. [54] by means of thermomechanical treatment (cold rolling then annealing). However,

the later sample showed much higher ductility of 30% uniform elongation and around 65% strain to failure versus only 2.1% strain to failure [45]. The reason behind these significant differences lies in the bimodal structure of the sample produced by Wang et al. i.e. the presence of the relatively large micro-sized grains with 25% vol. embedded within a matrix of nanocrystalline/ultrafine grains, which accounts for such superior ductility as well as the reduced strength in ref. [54] compared to that in ref. [45].

In contrary to what was mentioned in ref. [54] regarding the difficulty to process an artifact free bulk nc metal, Youssef, et al. [3] has achieved this using in-situ consolidation ball milling technique. The Cu powder was first cryo-milled (at liquid nitrogen temperature) for 3 hr, which allowed achieving high density of dislocation and smaller grain size, then the milling was resumed under room temperature for extra 6 hr. The product then came out in the form of spheres (8mm diameter), where the in-situ consolidation has taken place while milling at room temperature. The average grain size of the sample was 23 nm with a narrow distribution of the grain size, so the entire grains were in the nanocrystalline size range (<100 nm) as can be seen in Fig. 2.3. The prepared sample exhibited ultra-high yield strength of ~790 MPa (higher than [55]), and ultimate tensile strength of ~1120 MPa, along with microhardness value of 2.3 GPa. The sample has also shown a very good amount of ductility that reached 15.5% elongation to failure, as can be seen clearly in Fig. 2.4, thanks to the well consolidated artifact-free structure. BF-TEM image (Fig. 2.5) proved that there were dislocations piled-up at the GB, which also accounts for the high ductility and strain hardening shown in Fig. 2.5 [3], [51].

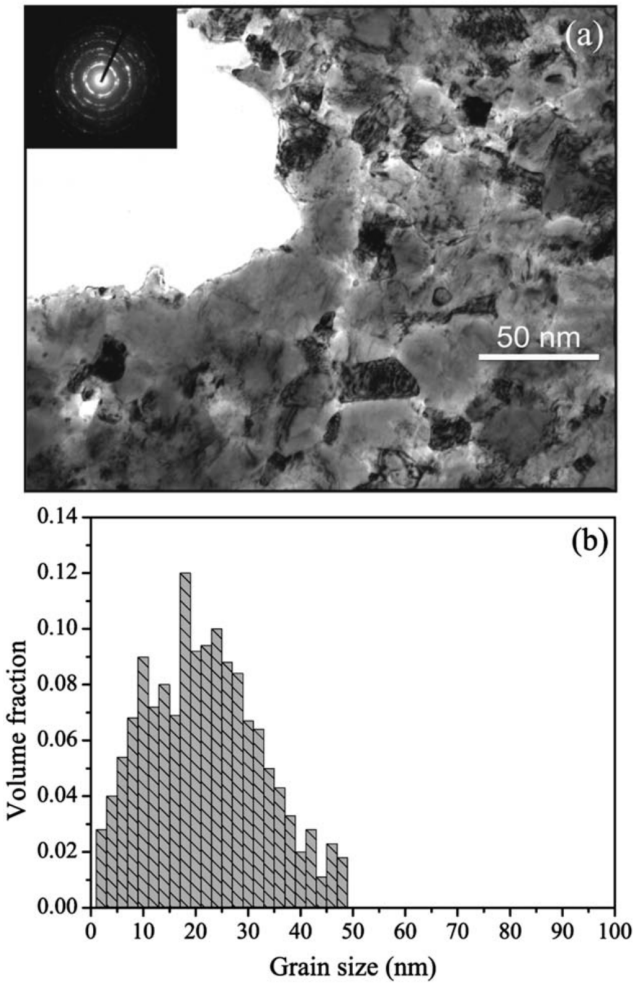

Figure 2.3 (A) BF-TEM micrograph of in situ consolidated nc Cu shows randomly oriented equiaxed grains, (B) Corresponding statistical distribution of the grain size [3].

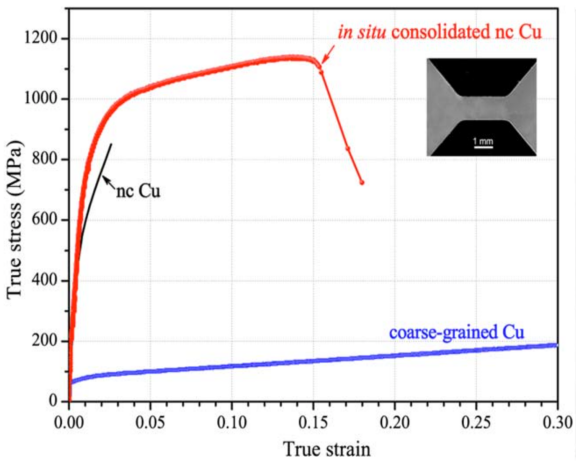

Figure 2.4 Tensile stress-strain curve for bulk nc Cu [3] compared to a CG polycrystalline Cu and a nc Cu prepared by inert-gas condensation [45].

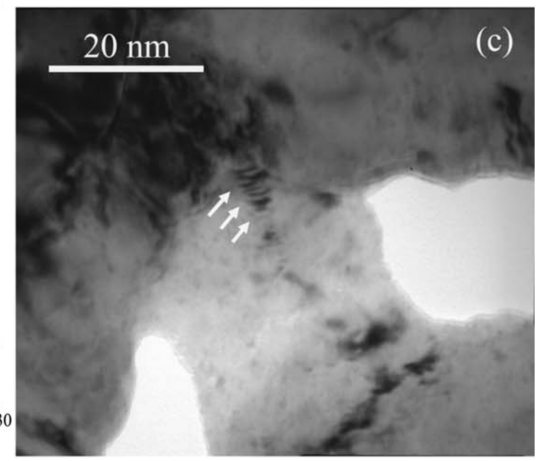

Figure 2.5 BF-TEM image of in situ deformed bulk nc Cu sample showing dislocation piles up at the grain boundaries [3]

Botcharova et al. [34] produced nc Cu-10 at.% Nb alloy via mechanical alloying. The alloy was then consolidated by hot pressing, and the final grain size was <50 nm. Mechanical testing showed a superior compressive strength of 1625 MPa, which is the highest reported value up to date for such an alloy. Again, this high compressive strength was mainly due to the grain boundary strengthening mechanism.

Özerinç et al. [58] revealed a hardness value of a thin film nc Cu-10 at.% Nb alloy, made by sputtering technique, to be more than 5 GPa. This value is more than double that of the pure nc Cu. They attributed this to the strengthening that came from the segregation of a solute with a large atomic size mismatch with Cu (i.e. Nb) to the GB.

Later, Abad et al. [30] studied the mechanical properties of nc Cu-15 wt.% Nb (10.8 at.% Nb), that was produced by mechanical milling for 30 hr, then consolidated using the high-pressure torsion (HPT) at ambient temperature. The sample exhibited a very high hardness of 6 GPa (Fig. 2.6), which is greater than a value reported by Mula et al. [39] for a similar sample. It was concluded from this study that increasing both the Nb content and the time of milling increases the hardness of the alloy [30]. Significant improvements in the mechanical properties of various nc metals/alloys have also been reported [2], [6], [7], [59]–[62].

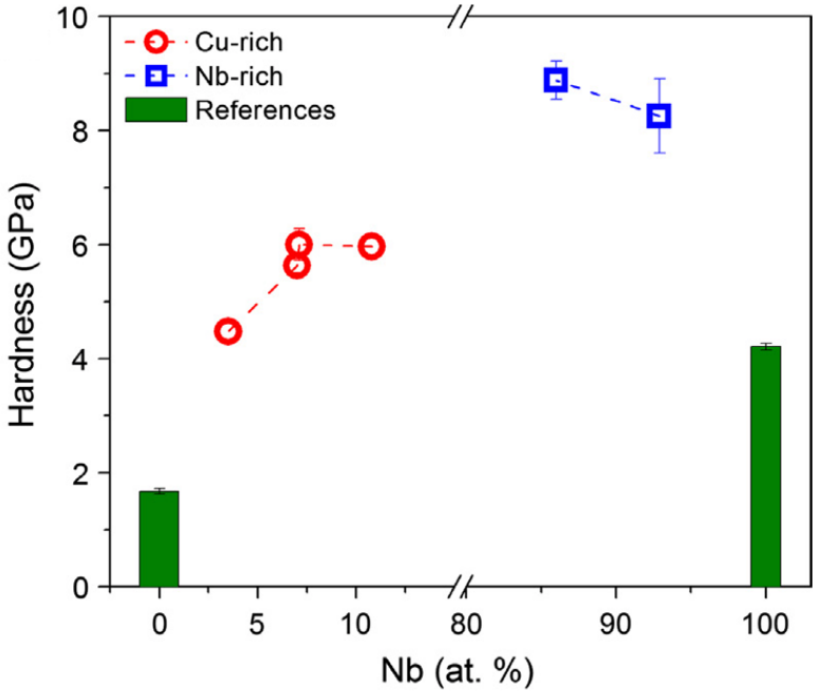

Figure 2.6 Variation of the hardness value of the nc Cu_xNb_{1-x} versus Nb content (at.%) [30].

2.2.2 Strengthening Mechanisms

Now it is clear that the nc metals and alloys possess a higher hardness and strength relative to their CG counterparts, but what is the main reason behind such behavior? The purpose of this section is to answer this important question. Earlier, in the 18th century, scientists did not know about the existence of a specific relation that relates a material's strength to its average grain size. However, they knew that the highest quality iron is the one with the smallest grain size. In the 1950s, and with the development of the electron microscopy, the observation of the dislocation defects was made possible. Hence, explaining many mechanical and physical phenomena. To comprehend the relation between the average grain size and the mechanical properties, let us consider the schematic drawing in Fig. 2.7 that represents two adjacent grains separated by a common GB. Normally, if a deformation is to take place, dislocation must move across this GB from A to B. Here, the GB will act as a barrier to this

movement due to two reasons, (a) the dislocation needs to change its direction due to the misorientation between the two grains, and this increases the difficulty of the crossing process; (b) there is an atomic disorder inside the GB itself, which produces a discontinuity in the slip planes between the two grains. Moreover, in a high angle grain boundary (HAGB) system, dislocation crossing the GBs might not be the case, rather, dislocations are more common to pile up at the GBs causing a stress concentration at the slip planes. This high stress may initiate the formation of new dislocations in the adjacent grains. A material with fine grains basically have more GBs, and hence, more obstacles for the dislocation motion during the deformation process. Therefore, nc materials possess higher hardness and strength [63].

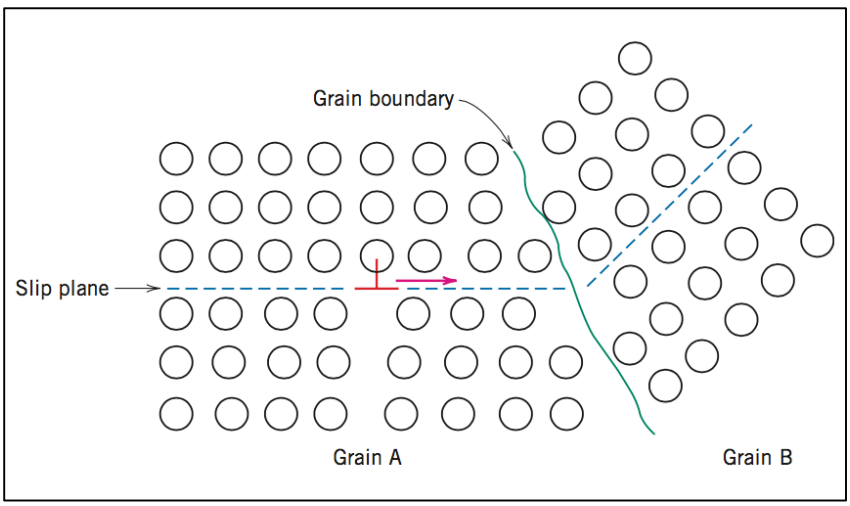

Figure 2.7 Schematic represents the dislocation motion within two grains A and B adjacent to each other and separated by a grain boundary [63].

E.O.Hall and N.J.Petch, got their hands on these findings and their research efforts helped them to achieve a mathematical relation between a material's strength and its grain size, which was named as "Hall-Petch relationship" after them, and it is as follows:

$$\sigma_y = \sigma_o + kd^{-1/2} \quad \text{Eq. 2.1}$$

Where σ_y is the yield stress, σ_o is the material's constant lattice friction stress needed to move one dislocation, also k is a material constant, and d is average grain size [64]. From the equation, it is obvious that as the value of the grain size (d) drops, the yield stress σ_y will increase, and hence the strength increase. Research work from the literature that emphasises the applicability of the Hall-Petch relationship to the nc materials can be found in [4], [21], [34], [54], [59], where the strength of these materials significantly increased with decreasing their grain size to the nano-range.

Aside to the grain refinement strengthening mechanism, strengthening from the solid solution have been also realized in nc materials [65]–[68]. The existence of solute atoms inside the lattice increases its frictional stress [69]. As per Youssef et al. [6], solid solution hardening had partially contributed by 11% to the total strength of the nc Al-5%Mg alloy. Equation 2.2 [70] describes the solid solution hardening as a function of the shear modulus of the mixture (G), the strain due to the misfit in the atomic size (ε), and the solute atomic fraction (c), and it is as follows:

$$\tau_{ss} = \beta G \varepsilon^p c^q \quad \text{Eq. 2.2}$$

Where β *is a constant,* and p and q are constants depending on the spacing between the solute atoms, and the interactions between the dislocations and these atoms.

2.3 Synthesis of Nanocrystalline Metals and Alloys

There are many different techniques to produce metals and alloys with nanoscale grain size. These techniques can be categorized under two main approaches; named bottom-up approach and top-down approach [71]. The bottom-up approach

requires starting from the atomic scale and constructing the nanostructure atom by atom, molecule by molecule, cluster by cluster. This approach includes many techniques such as, physical vapor deposition (PVD) [72], chemical vapor deposition (CVD) [73], pulsed electron deposition [74], inert gas condensation [75], spark erosion [76] and sputtering [77]. Meanwhile the second approach -as the name suggests- implies breaking down the bulk material into smaller pieces till reaching the nanoscale. This approach involves techniques such as lithography [78], ball milling, and other applications of severe plastic deformation [5]. However in the literature, lithography sometimes can be categorized under a third approach known as hybrid top-down and bottom-up approach [79]. The 1D and 2D nanostructured (ns) materials are typically synthesized using vapor or electrodeposition techniques, whereas the 3D ns materials are commonly achieved using either gas condensation or ball milling techniques [19].

The following section focuses only on ball milling technique, since it is used to produce nc materials in this thesis, revealing its advantages and disadvantages.

2.3.1 High Energy Ball Milling

There are two slightly different terms used to refer the processing of powder particle via ball milling, *Mechanical Milling* (MM) and *Mechanical Alloying* (MA). The first term is commonly used while dealing with a single pure metal powder, intermetallic, or an alloy that have been already prepared before being milled. On the other hand, the term MA is used to refer the process when different kind of metals/alloys are to be milled together so that a new homogenous material/compound is to be formed out of this milling process [80]. Another term is the *Cryomilling*, which implies milling under very low temperature using, for example, liquid nitrogen. This

technique is ideal for milling ductile metals [3], [4], [80]–[83].

High energy ball milling belongs to the top-down category, where nanomaterials are produced by milling the bulk material so that its conventional grain size decreases to the nanoscale due to the severe plastic deformation accompanying this process. This technique was firstly hosted by Benjamin et al. at the International Nickel Co. in 1966, and it was mainly used to make oxide dispersion-strengthened alloys (ODS). In this technique, the powder is loaded to a steel vial along with a specific number of steel milling balls. In the case of no oxides are intended to be formed, as in this thesis, the vial must be sealed using fixable 'O' ring within inert environment e.g. a glovebox filled with ultra-high pure argon gas. The vial is then placed in the milling machine. After starting the milling process, the vial starts to rotate in one direction, meanwhile, the balls rotate in the other direction as can be noticed in Fig. 2.8A [84]. the powder is then subjected to continuous collisions with the milling media (balls/vial) that causes it to be ground as can be shown in Fig. 2.8B. There are two kinds of collisions that happen inside, ball-powder-ball collisions and ball-powder-vial collisions [38]. What exactly happens inside the milling vial is a continuous and repeated fracture and cold welding processes in the grains of the powder. At the beginning of milling, the work hardening resulting from the collision causes the particles to fracture, forming new soft surfaces that have high tendency for agglomeration so it welds back again forming particles that are even bigger than the conventional size. After continuous milling, the particles get fractured by fatigue failure. Here the fracturing starts to take over the cold welding [80]. Severe plastic deformation happens at elevated strain rates causing the density of dislocations in the material being milled to increase. At critical dislocation density, the microstructured

material starts to break down into subgrains with low angle grain boundaries. With continuous milling, those subgrains evolve into final grains in the nanoscale with high angle grain boundaries, which eventually produces the aimed nano-sized structure [25].

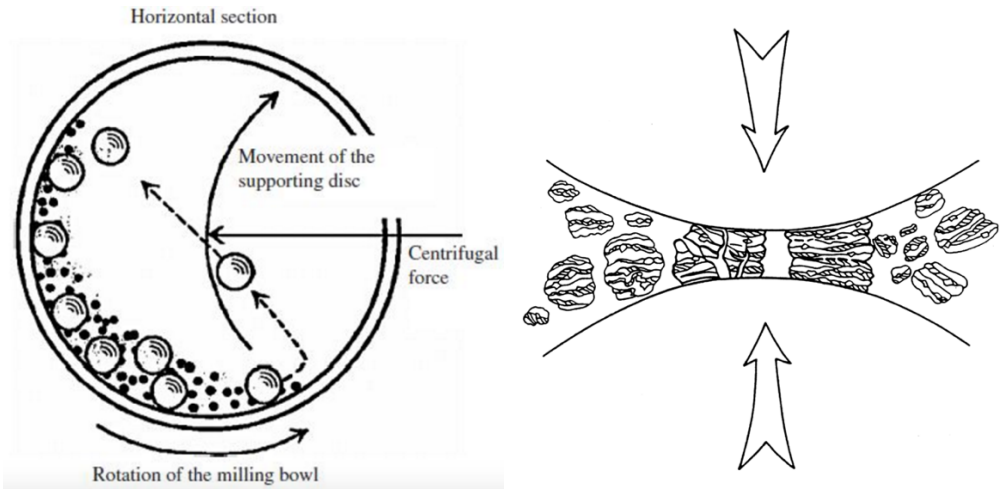

Figure 2.8 Schematic showing (A) the movement of the balls and the vial [84], (B) the grinding mechanism between two balls [85].

There are many parameters that control the milling process, including but not limited to; milling temperature, milling time, milling speed, the milling atmosphere, and ball to powder weight ratio (BPR). Generally speaking, the higher the BPR, the less time is required to achieve the minimum grain size [80]. MM/MA has been used to produce many materials such as iron/iron alloys [86],[87], copper/copper alloys [21], [26], [30], [32], [81], [88], [89], aluminum/aluminum alloys [8], [61], [90], [91], and magnesium/magnesium alloys [7], [62].

2.3.2 Advantages and Disadvantages of Ball Milling

One key advantage of MM/MA technique is that it offers an economic method to synthesize nanomaterials, which is relatively cheaper than other techniques (e.g.

sputtering). It also operates at normal temperature, unlike other techniques that require relatively higher temperature, especially when it comes to the formation of intermetallics [85]. Another advantage is the possibility of mass production using this technique, so it can be used on an industrial scale. Moreover, MA/MM is a non-equilibrium process, which enables the production of non-equilibrium phases that are impossible to be produced using the other equilibrium methods. Thanks to the vast areas at the grain boundaries that are available for segregation, the saturation of the element(s) in the alloys can be increased beyond the conventional saturation limit. Hence, creating supersaturated solid solutions [80], [92]. In addition to this, the possibility to use cryogenic milling for soft and ductile metals/alloys will permit achieving the lowest possible grain size in the nano-range. Since the very low temperature will help to embrittle the metals and decrease their tendency for cold welding [80].

In spite of these advantages, MM/MA still has some drawbacks. The major drawback of this technique is contamination. The main source of contamination is Fe, which is introduced to the powder from the milling media. High Fe contamination (>5%) was noticed in high energy mills (e.g. Spex shaker mill) over prolonged milling hours. A possible solution is to replace the steel milling media with another one made of transformation-toughened zirconia/tungsten carbide. Oxygen is also a source of contamination, which can be eliminated or minimized by using an inert gas as stated in the previous section. Another difficulty may arise while milling ductile metals/alloys, as they tend to pile up on the walls of the vial and around the balls. Though surfactant may be used to solve this issue; yet its decomposition will add to the contamination of the system [85]. Hence, cryomilling is a better solution to avoid welding.

2.4 Thermal Stability in Nanocrystalline Materials

As discussed in section 2.2, decreasing the grain size to the nanoscale range results in exceptional properties in the materials. Consequently, maintaining these properties is only possible through preserving such very small grain size. Unfortunately, nc materials are not thermally stable, as their gains start to grow back to their original size at temperatures as low as room temperature, hence losing its nanostructure, and the superior mechanical properties as a result [18], [19].

Searching for a solution to this problem is very important not only for the scientific aspect but for the industrial and technological aspects as well. As for the industrial level, and since most of the techniques produce the nc materials in the shape of tiny particles, synthesis bulk nc materials requires the consolidation of such particulates, which often happens at high pressures and temperatures. Accordingly, grain growth will always be a problem in such cases. The target is to achieve a 100% dense bulk nc material out of these particulates with minimal or zero grain growth. Hence the proper understanding of the grain growth is the key to solve this problem. This shall be validated through studying the stability of both the microstructure and the GBs' structure.

2.4.1 Grain Growth

Grain growth up to double of the initial nc grain size has been observed in some nc pure metals with melting temperatures less than 600 °C, such as Al, Mg, Pb, and Sn, within just 24 hours at room temperature [93]. The reason behind the grain growth in such materials is that they have a high volume fraction of GB regions, therefore more atoms occupying interstitial positions, which is unfavorable energy wise [94], [95].

Since the overall energy of the system is now unfavorably high, and as any system, tends to lower its energy, the only way to do so is to decrease the area of the GB region, and as for pure elements, this can only be achieved via grain growth. This can be understood from the relationship that relates the change in the area of the grain boundary (dA) to the change in Gibbs free energy (dG)

$$dG \propto \gamma dA \qquad \text{Eq. 2.3}$$

Where γ is the surface free energy of the GB per unit area. The grain growth in pure nc metals is very significant, since the elemental metal has a positive GB energy. Therefore, lowering its Gibbs free energy will be on the expense of reducing the interfacial spacing between its grains, i.e. increasing the grain size [96]. Therefore, decreasing the interfacial free energy is the driving pressure for this growth process, consequently, reducing the free energy of the whole system. The growth of the grains can be considered as an enlargement in the curved interface because of a driving pressure (P) that keeps pushing this interface, where this pressure can be described as:

$$P = \alpha \frac{\gamma}{r} \qquad \text{Eq. 2.4}$$

Where α is a constant and r is the GB radius. It is obvious form equation 2.3 that a smaller GB radius (r) produces higher driving force (P) for the grain growth. Such driving force can reach up to 1 GPa for a grain size of 10 nm, [8], [97].

Darling et al. [97] examined the effect of elevated temperature on pure nc copper prepared by electroplating. The sample was annealed to 64% of the melting point (T_m) of Cu for 2 hr. TEM observations (Fig. 2.9A and B) confirmed a severe grain coarsening from an average grain size of 60 nm to 60 μm, which is a thousand times increase!

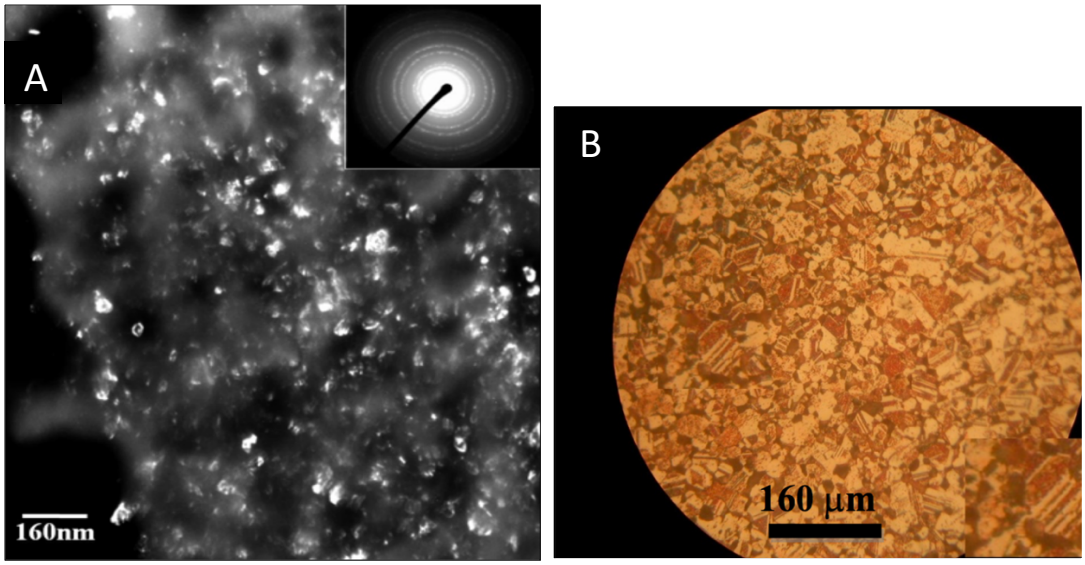

Figure 2.9 Images of the microstructure of nc copper (A) as deposited by electroplating, (B) after sintered at 600 °C for 2 hours [97].

Other many research efforts have been conducted as to show the influence of temperature on the stability of the grains in pure nc metals like Cu, Ni, Mg, Al, Zn, and Pb, which experienced grain growth at low temperatures [96], [97]. Fig. 2.10 shows the effect of the reduced annealing temperature (T/T_m) on the grain size of various pure nc metals [28], [86], [98], [99]. It is obvious from this Figure that the grains kept growing with the increase of the annealing temperature, which indicates that grain growth is a general problem that faces many nc metals. Hence, finding a solution to such a problem is of an utmost importance.

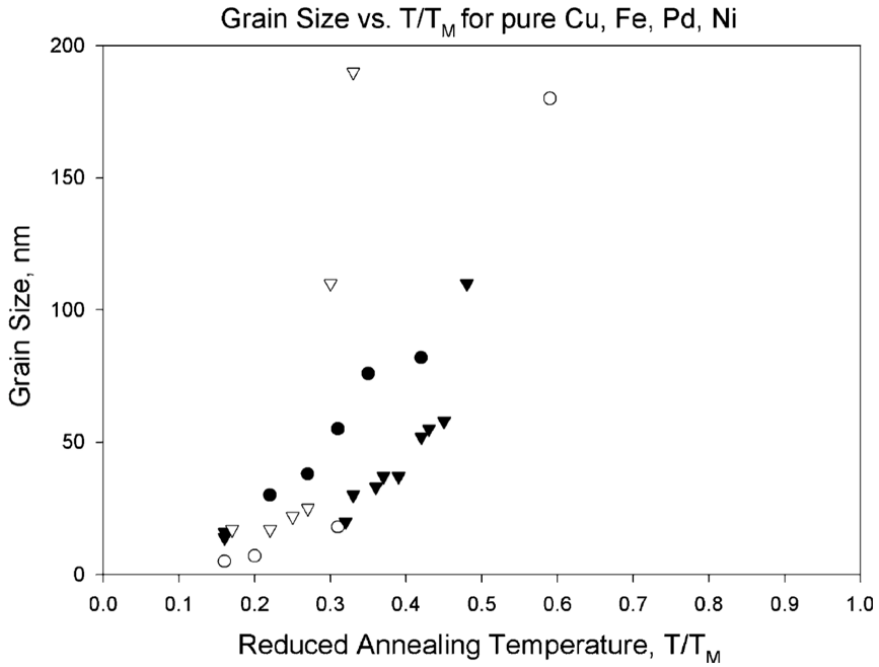

Figure 2.10 Graph exhibiting the trend of grain growth for different pure metals denoted as: Cu ●, Fe▼, Pd ○, and Ni ▽ [28].

2.4.2 Thermal Stabilization Approaches

Two main approaches are reported in the literature to surmount the thermal instability issue in nc materials: Kinetic Approach and Thermodynamic Approach. These approaches emerged from equation 2.5 which describes the velocity of a GB experiencing grain growth as a function of its mobility (M) and the driving pressure (P) [100]:

$$v = M.P = M_o \exp(\frac{-Q}{RT}.\frac{2\gamma b}{r}) \quad \text{Eq. 2.5}$$

Where M_o is the mobility pre-exponential factor, Q is the activation energy, R is the universal gas constant, and T is the absolute temperature. From the equation, we can tell that for nc materials at low temperature, there is still sufficient GB velocity since the very small r compensates for the low mobility that exists at lower temperatures [101]. Additionally, to prevent or minimize grain growth, we either have to lower the

mobility (M) by pinning the GB in place or to reduce the driving force (P). It is quite important to mention that both approaches involve introducing some foreign atoms to the system. Hence all the reported nc systems, up to date, are not pure elements [28]. This highlight how the instability issue of the nc materials has limited their usage in the technological applications which might take advantage of their inherent properties as of being pure metals. This is because alloying and/or the existence of impurities severely affect(s) some of the original excellent properties.

2.4.2.1 Kinetic Stabilization Mechanisms

In the Kinetic approach, the mobility of the GBs is controlled by different mechanisms, including: solute drag [102], second phase drag (Zener pinning) [103], porosity drag [104], and chemical ordering [105], [106]. The first mentioned two mechanisms are the most important ones in this thesis, so we shall discuss them in details.

2.4.2.1.1 Solute Drag Effect

The growth of the grains depends on the possibility of the boundary to skip the solute atmosphere. Two opposing forces controlling such possibility: (1) the magnitude of the drag force, and (2) the driving force of the grain growth. The magnitude of the drag force can be understood by studying the effect of solute concentration on the mobility of the GB. It was believed that at low solute concentrations, mobility does not significantly change, and grain growth takes place. However, increasing the solute atoms makes it more difficult for the boundaries to move and expand, i.e. the higher the amount of solute, the lower the mobility of the GB. Hence, more thermal stability

for the system will be possible. Meanwhile, when the driving force of grain growth is low, the solute atoms will have sufficient time to diffuse and hinder the GB mobility. However, with the increase of this force, as in the case of the nc materials, grain growth will be faster; hence the solute atoms have to diffuse through larger areas in less time. Solute drag may still be effective at high temperature, due to the enhanced diffusivity of the thermally expanding lattice. However, it should be noted that the value of the pinning force will depend on the interactions between the solvent and the solute [25], [97].

Michels et al. [102] investigated the thermal stability of the annealed Pd-19 at.% Zr alloy at 600 °C for 30 hr. They noticed an increase in the average grain size from 5 to 16 nm, and that the average concentration of Zr atoms at the GBs has increased from 19% to 26.5%. They claimed two possible approaches may describe this behavior. Either the GBs have trapped the Zr atoms while growing (solute drag), or that these atoms have diffused to the GBs through the lattice. However, since the 600 °C only represents 0.47 of the melting temperature for this alloy, the diffusion approach is less likely to be validated. Hence, solute entrapment is the logical approach here to account for the increase of the Zr concentration at the GB areas. VanLeeuwen et al. [107] studied the same system at even higher temperatures and concluded that the thermodynamic approach cannot describe the scenario since the decrease in the energy of the GB due to the segregation is not enough to prevent the grain growth, as can be seen in Fig. 2.11, which demonstrates the occurrence of severe grain growth after annealing at 950 °C. Meanwhile, the solute drag could stabilize the system up to 700 °C. The same interpretation was made for a Ni-1 at.% Si alloy, where the stabilization was achieved due to the entrapment of the Si atoms between the GBs (solute drag

mechanism) [108], hence proving that even low solute additions still have the ability to hinder the GB motion.

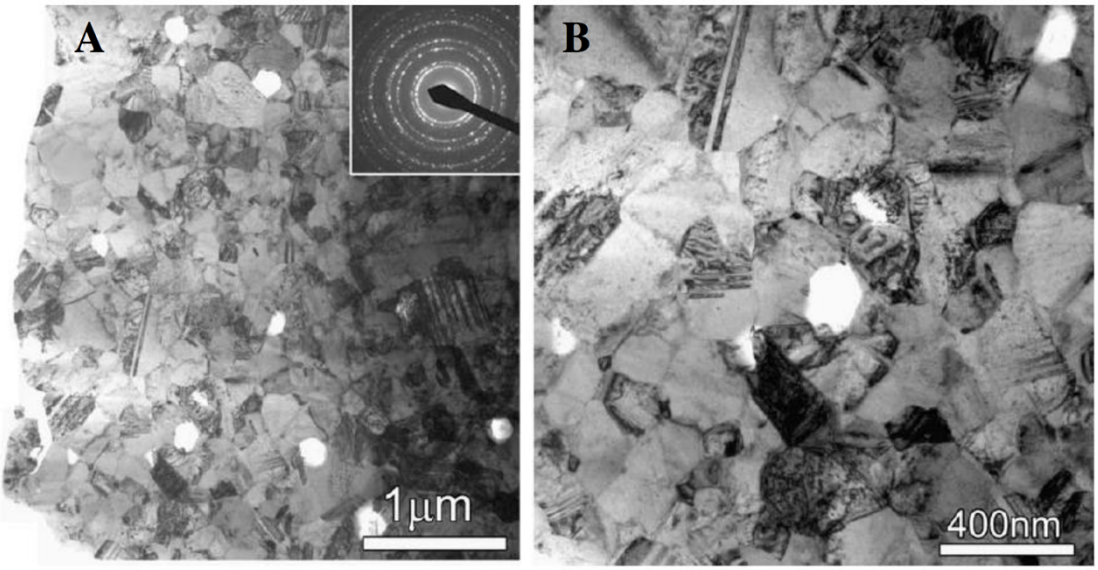

Figure 2.11 TEM images exhibit the microstructure of Pd-19 at.% Zr alloy annealed at 950 °C for 1 hr. (A) low resolution, (B) high resolution [107].

2.4.2.1.2 Second Phase (Zener) Pinning

Again, as mentioned before, all the stabilization mechanisms imply introducing foreign solute atoms to the system. If these atoms formed a second phase either as precipitates or dispersoids, where they hinder the movement of the GBs, then it is said to be Zener pinning/effect or the second phase pinning as can be understood from the following equation:

$$P_z = \frac{3F\gamma}{2r} \qquad \text{Eq. 2.6}$$

Where P_z is the pinning pressure exerted by the dispersoids or the precipitates, F is the volume fraction of the particles with radius r, and γ is the GB interfacial energy. For the sake of having good thermal stability, the P_z in Eq. 2.6 should be more than or comparable with the driving pressure (P) in Eq. 2.4. Hence a high volume fraction of

the second phase particles and/or an extremely small radius are/is needed. It is worth mentioning that the Zener pinning has a lower sensitivity regarding the high temperature than the solute drag. Thus, it is more effective to impede the motion of the GB at relatively higher temperatures [109].

Shaw and his co-workers [91] examined the thermal stability of the mechanical alloyed $Al_{93}Fe_3Ti_2Cr_2$ alloy. They achieved thermal stability up to 77% of the melting point of this alloy, where a very limited grain growth occurred to the FCC-Al grains, as some of them remained in the range of 20 nm. They attributed the initial stability to the solute drag mechanism with some possible contribution from the second phase drag (Zener). However, for the stability above 450 °C (0.77 T_m), it was mainly due to Zener mechanism where the formation of the intermetallic compounds such as Al_6Fe, followed by Al_3Ti, $Al_{13}Fe_4$, and $Al_{13}Cr_2$, has taken place and contributed to the stabilization of GBs.

Zener effect was successful to stabilize nc Cu system, as in the case of using solutes of W [110], Mo [111], or Nb [32], [33]. In a recent work, Atwater et al. [26] found that only 1 at.% Zr was able to thermally stabilize nc Cu prepared by cryomilling up to 900 °C. They attributed such stability to the second phase pinning mechanism, where the precipitation of ZrO_2 and Cu_5Zr particles appeared to be enough to account for the thermal stability of this system. As illustrated in Fig. 2.12, the two FCC-Cu outermost SAD rings reveal an average grain size of ~60 nm, meanwhile, the two innermost rings give an indication of the average grain size of the second phase particles which appears to be 5-10 nm.

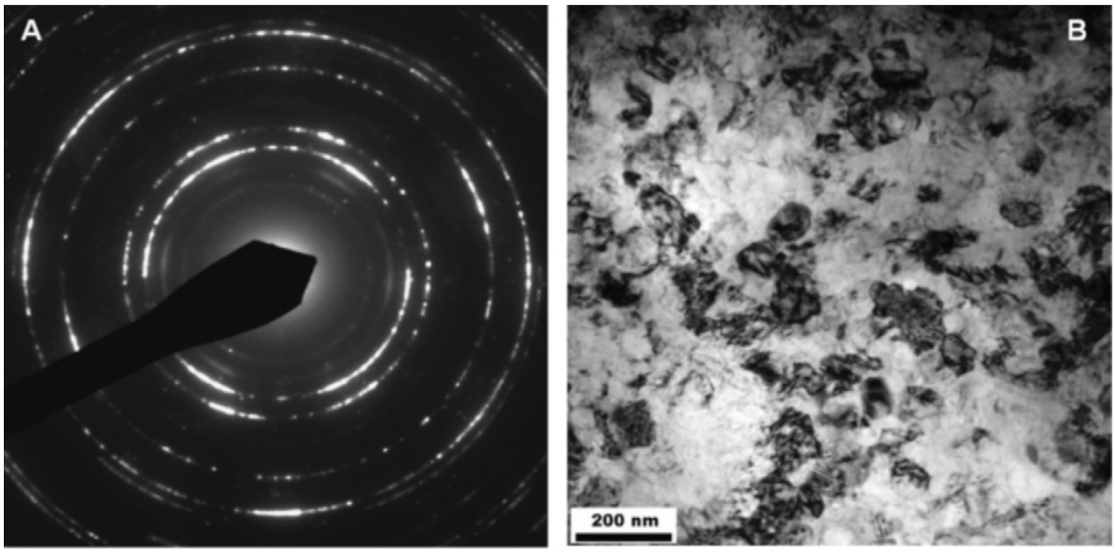

Figure 2.12 (A) SAD pattern, (B) BF-TEM image of the cryo-mechanical alloyed nc Cu-1 at.% Zr annealed at 900 °C for 1 hr [26].

A very recent study was conducted by Lei et al. [38] on a mechanical alloyed nc Cu-10 wt.% Nb. It was found that the Nb particles grew to about 10 nm, and the Cu remained below 100 nm even after annealing at 900 °C for 3 hr. This was evidenced from the bright field TEM micrographs shown in Fig. 2.13. The Hardness value decreased from 460 HV for the as-milled to 375 HV after annealing, which is still relatively high. This high stability was mainly due to the solute drag (at lower temperatures) as well as the pinning effect that was more significant at the higher annealing temperatures.

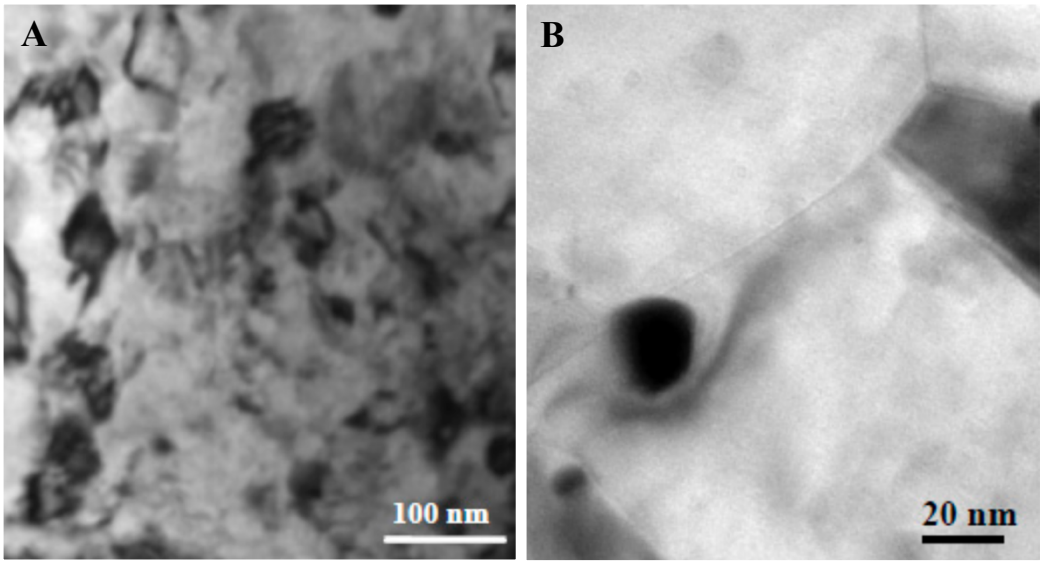

Figure 2.13 BF-TEM of nc Cu-10 wt.% Nb annealed at 900 °C for 3 hr, (A) Cu nano-grains, (B) Nb nanoparticles [38].

2.4.2.2 Thermodynamic Stabilization Mechanisms

By reference to Eq. 2.5, that describes the velocity of GB as the multiplication of the mobility (M) and the driving force (P), $v = M.P$, we have already mentioned the kinetic stabilization approach that aims to lowering the "M" term. However, the thermodynamic approach aims to lower the other term "P". In other words, the thermodynamic approach works on the reduction of driving force of the GBs by lowering their Gibbs free energy. Solute atoms should be able to easily segregate to the GBs filling the gabs and reducing its free energy [28]. Solving the Gibbs adsorption equation leads to a relation between the solute content and the reduction in the GB energy, which is stated in Eq. 2.7 below:

$$d\gamma = -\Gamma_A d\mu_A \qquad \text{Eq. 2.7}$$

where Γ_A is the segregated amount of solute to the GB, and μ_A is the chemical potential of the species (solute atoms) [112]. From Eq. 2.7 we can tell that, the more the segregated solute atoms to the GB, the more reduction in the GB energy. Taking

into account that the larger the atomic size misfit between the solute and the solvent atoms, the higher the tendency for the solute atoms to segregate to the GB. This is mainly because of the need for such bigger atoms inside the ordered lattice to release its high elastic strain by moving to the empty spaces that present inside the disordered GB region. High temperature also promotes such solute segregation. This process shall reduce the GB energy, which is the driving pressure for the grain growth (P) (see Eq. 2.5), and eventually thermally stabilize the system [113]. This concept have been used by Weissmüller [114], [115], Kirchheim [20], [116], and Millett [92]. The first trial to solve the Gibbs adsorption isotherm was made by Weissmüller [114], [115]. It described the GB energy after the segregation as follows:

$$\gamma = \gamma_o + \Gamma_s \left[\Delta H_{seg} - T\Delta S_{seg}\right] \quad \text{Eq. 2.8}$$

Where γ is GB energy after segregation, γ_o is the energy of the non-segregated GB, and ΔH_{seg} and ΔS_{seg} are the differences in the enthalpy and entropy after and before segregation, respectively. Based on Eq. 2.8, in order to obtain a "γ" that is lower than "γ_o", it is required that the value between the two brackets, $[\Delta H_{seg} - T\Delta S_{seg}]$, to be as negative as possible. Earlier, McLean [117] stated that the change in the enthalpy of segregation, ΔH_{seg}, comes solely from the release in the elastic strain energy. On the other side, Defay et al. [118] reported that this change in enthalpy is only due to the chemical interactions. In fact, both of them were not completely true, since ΔH_{seg} should involve the two parts; the chemical contribution (ΔH_{chem}) resulting from the solute solvent chemical interaction, and the elastic strain contribution (ΔH_{els}) as a result of the atomic size misfit of the solute/solvent atoms. This was summarized by Wynblatt-Ku [119], [120] in their model as in the following equation:

$$\Delta H_{seg} = \Delta H_{\text{chem}} + \Delta H_{\text{els}} \quad \text{Eq. 2.9}$$

Friedel [121] came out with an equation that can calculate the value of the ΔH_{els} as below:

$$\Delta H_{els} = - \Delta E_{els} = \frac{2K_B G_A (V_B - V_A)^2}{3K_B V_A + 4G_A V_B} \quad \text{Eq. 2.10}$$

Where ΔE_{els} is the total released elastic strain energy, K is the bulk modulus, G is the shear modulus, and V is the molar volume of solute A and solvent B. There are many models that explain the thermodynamic stabilization and the segregation process. However, the following part shall discuss the two most famous ones, Kirchheim's models [20], [116], and the more recent, Trelewicz and Schuh [96].

2.4.2.2.1 Kirchheim's Model

Kirchheim inspired this model from the earlier model of Weissmuller [114], [115]. He accounted for the equilibrium area of the GB and its change with the temperature. As it can be deduced from Eq. 2.3, assuming positive GB energy, grain growth will occur to lower the free energy of the system. This grain growth is eliminated only when "γ" is equal to zero. The equilibrium grain size (diameter of a grain at saturation) of a high segregation enthalpy alloy with a very low solubility limit can be deduced from Eq. 2.10 [82]:

$$D = \frac{3\Gamma_s^* V_{AB}}{X_A^0} \quad \text{Eq. 2.11}$$

Where Γ_s^* is the solute excess corresponding to the saturated GB monolayer, X_A^0 is the total solute concentration at the bulk and the interface, and V_{AB} is the molar volume. This equation exhibits the inverse relation between the equilibrium grain size and the solute content. This model claims that in a saturated GB, two behavior compete; precipitation and segregation. However, precipitation shall cause a lower energy state

in systems with strongly segregating solute atoms [116]. Kirchheim [122] considered the GBs, dislocations and vacancies as defects. He examined the reduction in energy that accompanied the formation of such defects in [122], [123], which was later modeled by Millet et al. [124]. as a reduction in the excess free energy to zero in order to estimate the equilibrium grain size.

2.4.2.2.2 Trelewicz and Schuh (TS) Model

All the previous models made by Weissmuller, Kichheim, and Liu have a common limitation that they are only applicable in systems that contain dilute solution and a small volume fraction of GB. This is basically not the case in the nc materials, where there is a high amount of GB regions and the segregated solute to the GB can be high. Trelewicz and Schuh tried to overcome this limitation and came up with a model that can be applied on systems with either low or high segregating solutes. The model divides the binary alloy system into three regions: bulk, intergranular, and transition regions, as demonstrated in Fig. 2.14.

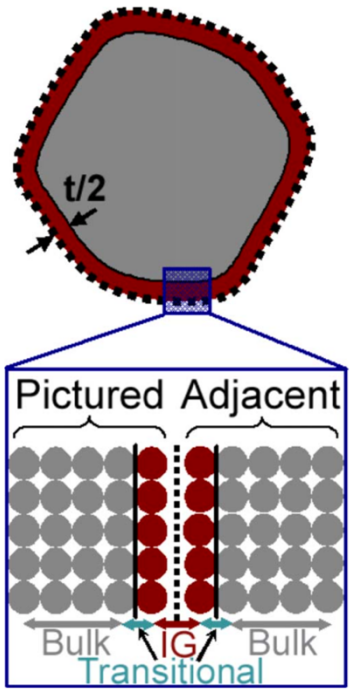

Figure 2.14 schematic showing two adjacent grains with the bulk region (gray), separated with an intergranular (IG) region (red), with a transitional region (cyan) that connects the IG and the bulk regions [96].

According to this model, the change in the internal energy (ΔU) needs to be calculated as the summation of the total energy of all the atomic bonds within each region. This ΔU arises due to the solute-solvent chemical interactions. After that, the mixing enthalpy (ΔH) is calculated using the value of the previously calculated ΔU. Considering an ideal solution, the mixing entropy (ΔS) is obtained and the Gibbs free energy (ΔG) is calculated in terms of ΔH and ΔS. Finally, ΔG is diminished with respect to the change in the concentration of the solute at the GB and the GB volume fraction. Solving all these equations leads to the equilibrium GB volume fraction, which shall eventually give the metastable equilibrium grain size. A relation between the energy of GB and the global solute content is plotted in Fig. 2.15A, as well as a relation between the grain size, solute volume fraction, and the annealing temperature (Fig. 2.15B).

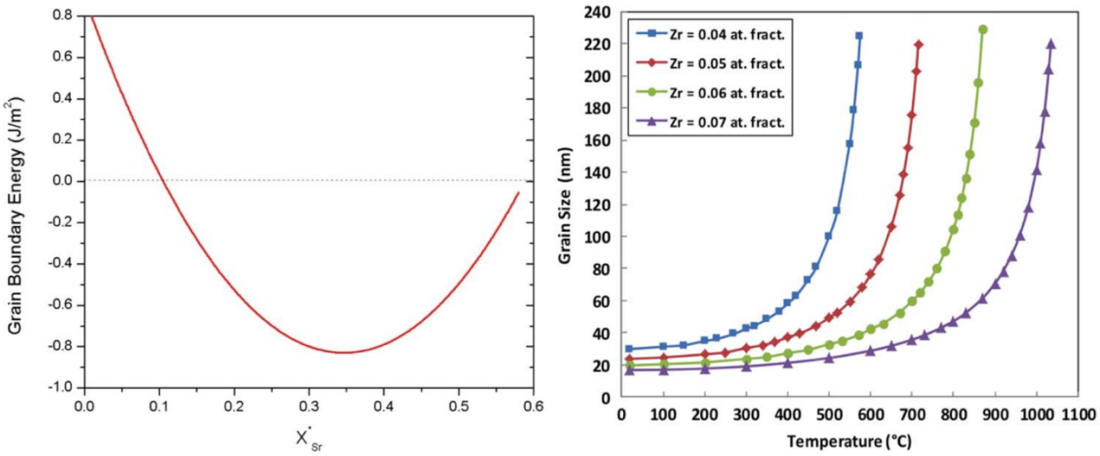

Figure 2.15 (A) GB energy vs. the atomic fraction of Sr in Al-Sr system [8], (B) Grain size vs. temperature at different concentrations of Zr in FeZr system [113].

Unfortunately, the TS model has some limitations. One of the limitations of this model is that the ΔH here has accounted only for the chemical contributions and did not account for any elastic strain contributions that are induced by the solute-solvent atomic size misfit. Another limitation is that this model assumes no formation of any secondary phase, hence it cannot be applied where the formation of precipitates is possible. Even though this model suffers from the mentioned limitations, yet it provides better interpretations that match quite well with the experimental data, as it can be noticed in Fig. 2.16, where the grain size is plotted against the total concentration of solute in a high segregation system such as Ni-P system [125], and in a low segregation Ni-W system [126].

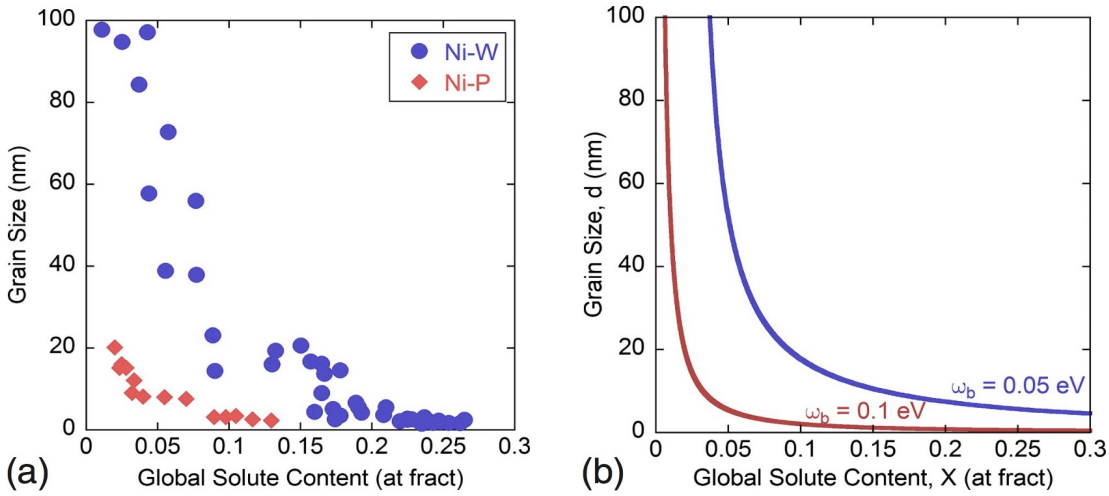

Figure 2.16 Grain size vs solute content for Ni-P [125] and Ni-W [126] systems as per the (a) experimental data, and (b) TS model [96].

Chookajorn et al. [127] have implemented some modification on the TS model by adding the contributions of the elastic strain to the change in the enthalpy. The new model generates nanostructured stability maps, where the mixing and the segregation enthalpies are plotted against each other. Fig. 2.17 shows the stability map of the tungsten alloys. This map can tell the ability of different solutes to stabilize nc tungsten. For example, the model here tells us that solutes like Zn, Ti, or Mn can stabilize nc W system, whereas solute like Cu, Ag, or Cd cannot stabilize this system.

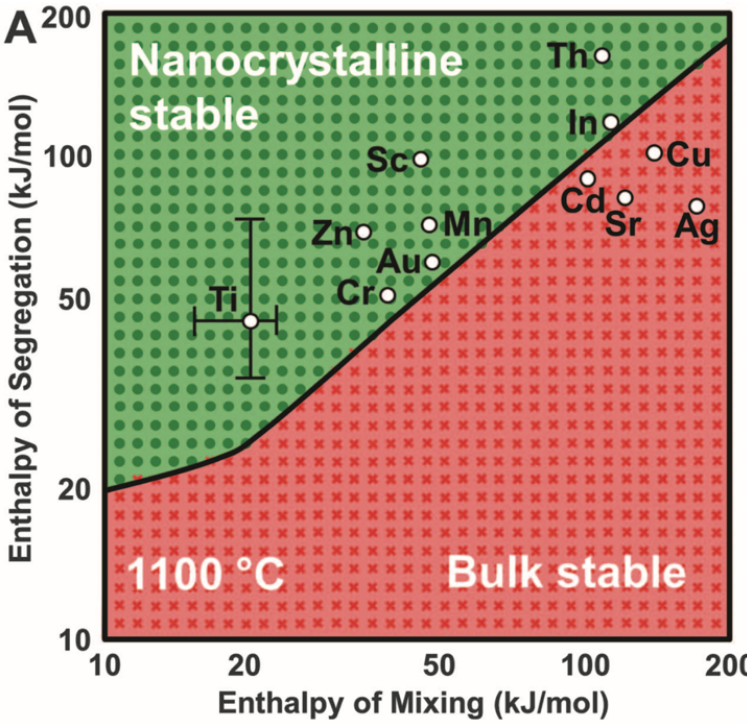

Figure 2.17 Stability map for nc W system, showing some of the elemental solutes that can and others cannot stabilize this system [127].

CHAPTER 3: EXPERIMENTAL WORK

This chapter introduces the experimental procedure that has been done in this thesis. The procedure is divided into two main parts; the first part represents the sample preparation process including the synthesizing process of nc Cu and nc Cu-1 at.% Nb via Mechanical Milling/Alloying (MM/MA), the annealing process at various temperatures to test its thermal stability, and finally the compaction and polishing of the samples in order to perform analysis using different characterization tools. The second part introduces the different characterization techniques that have been used to analyze the produced samples. This includes X-ray diffraction (XRD), transmission electron microscopy (TEM), Vickers microhardness tester, Tensile testing machine, Scanning Electron Microscopy (SEM), and the Four-Point Probe technique.

3.1 Sample Preparation

3.1.1 High Energy Ball Milling

Synthesis of nc Cu-1%Nb was performed using the mechanical alloying technique. Two elemental powders have been used: Cu and Nb with purities of 99.9% and 99.99%, respectively (purity obtained from Alfa Aesar®). They were all packed and sealed under argon, then opened and stored inside a glovebox, mBRAUN, (Fig. 3.1). Both humidity and oxygen levels inside this glovebox were <0.5 ppm. To produce pure nc Cu, the copper powder was inserted into a stainless-steel vial along with 32 stainless-steel balls (440C martensitic), the ball-to-powder mass ratio (BPR) was 8:1. In order to avoid contamination, the vial was well sealed under this ultrahigh purity (UHP) argon atmosphere inside the same glovebox. The vial was then mounted inside a high-energy ball miller (SPEX 8000M Mixer/Mill, Fig. 3.2), and milled for 8 hr at

room temperature (~18 °C). However, to produce nc Cu-1%Nb, 1 at.% of niobium powder was added to the copper powder. The exact same procedure was done as in the case of the pure Cu, then samples were milled for various milling hours; 1, 3, 5, 8, and 10 hr. A detailed description of how the powder was transferred into nano-sized grains was mentioned in section 2.3. The milling process is represented in Fig. 3.3. After the milling was completed, the product was collected in glass vials as in Fig. 3.4, and preserved inside the glovebox for the time of the analysis to keep the sample fresh, and minimize the risk of contamination.

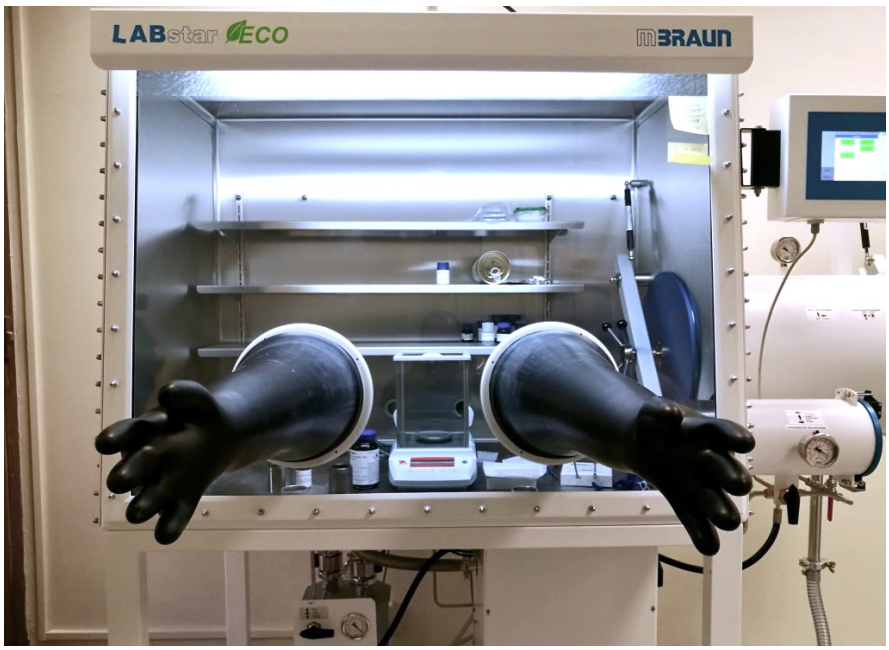

Figure 3.1 mBRUAN glovebox.

Figure 3.2 SPEX 8000M Mixer/Mill.

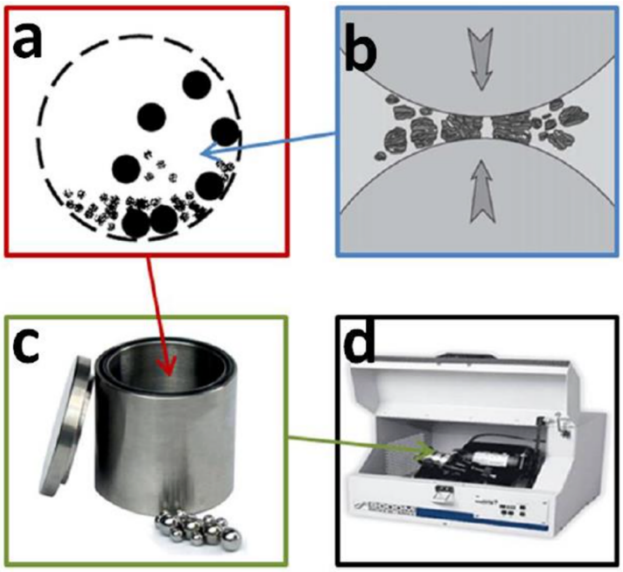

Figure 3.3 Schematic representation of the milling process [8].

Figure 3.4 Produced sample after milling.

3.1.2 Sample Annealing

Annealing of the nc Cu and Cu-1%Nb samples was performed in a tube furnace (MTI GL-1500, Fig. 3.5) under the flow of UHP argon (99.999%). A vacuum ($3*10^{-3}$

Torr) was applied and argon gas was flushed into the tube for three times. The samples were annealed at various temperatures for 1 hr. The cooling and heating rates were 10 and 5 °C/min, respectively.

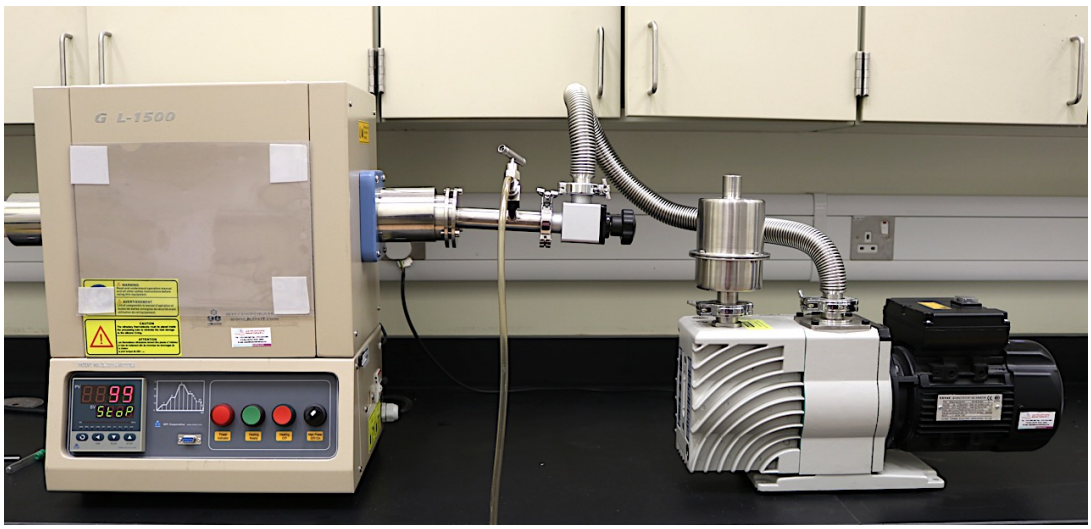

Figure 3.5 MTI GL-1500 tube furnace (on the left) attached to a vacuum pump (on the right).

3.1.3 Sample Consolidation

In order to perform characterization tests like XRD and microhardness tests, the samples must be compacted to a disk-like shape, as the XRD test requires a sample with a flat surface, and the microhardness test requires consolidation to the theoretical density and a smooth flat surface. About 3 g of each sample were loaded into a 6.35 mm die made of tungsten carbide (Fig. 3.6A), then an axial load of 2 GPa was applied on the punches using a cold mounting press (Carver, Fig. 3.6B). The result was a compacted ~1 mm disk specimen (Fig. 3.6C). To polish the disk, it was glued to a small bulk cylindrical glass, which was inserted in the middle of a steel die on a movable base. This base can adjust the elevation of the glass piece with the sample above by using an Allen key, see Fig. 3.6C. All the disks were polished using a Metkon Forcipol

grinder/polisher. Finally, they were mirror polished with a cloth and 0.05 μm alumina, using the same Metkon device.

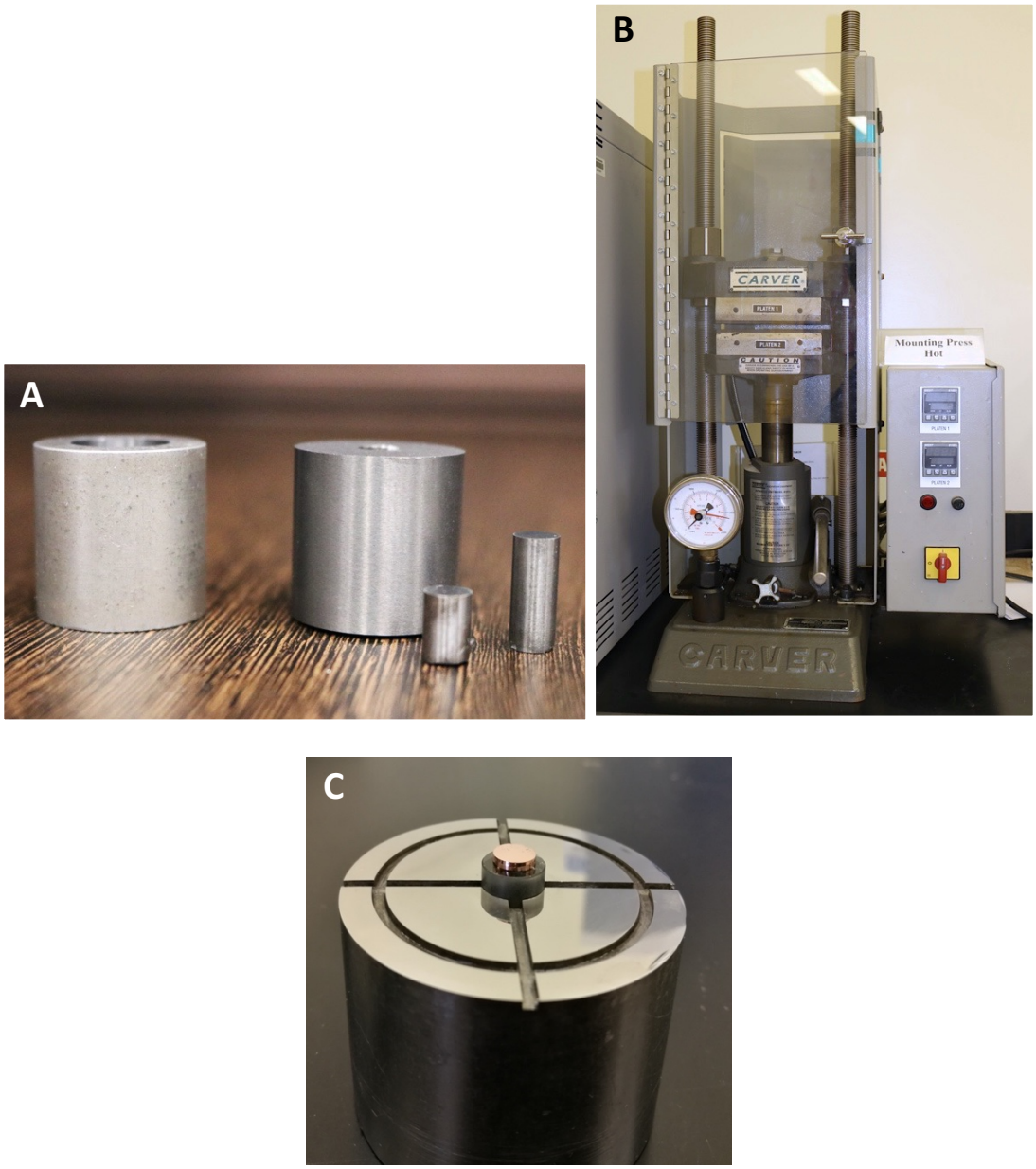

Figure 3.6 (A) From left to right; eject tool, die, and punches. (B) Carver mounting press. (C) Steel die along with the glass piece and ~1 mm sample disk above them.

3.2 Characterization Methods

3.2.1 X-Ray Diffraction (XRD)

X-ray diffraction analysis is one of the fundamental non-destructive techniques that is used to determine the crystal structure. In addition, many other crystal structure parameters such as the degree of crystallinity, grain size, inter-planar spacing, and lattice parameter and strain can be determined by XRD technique. The principles of XRD emerges from Bragg's law (Eq. 3.1) [128], which states that the path difference between the two incidents and the scattered waves ($2dsin\theta$) equals to multiple of x-ray wavelength, where a constructive interference has taken place. This can be derived from Fig. 3.7.

$$n\lambda = 2dsin\theta \qquad \text{Eq. 3.1}$$

Where n is the diffraction order, λ is the wavelength of the incident X-ray beam, d is the distance between two crystal planes (inter-planar spacing), and θ is the incident/reflection angle.

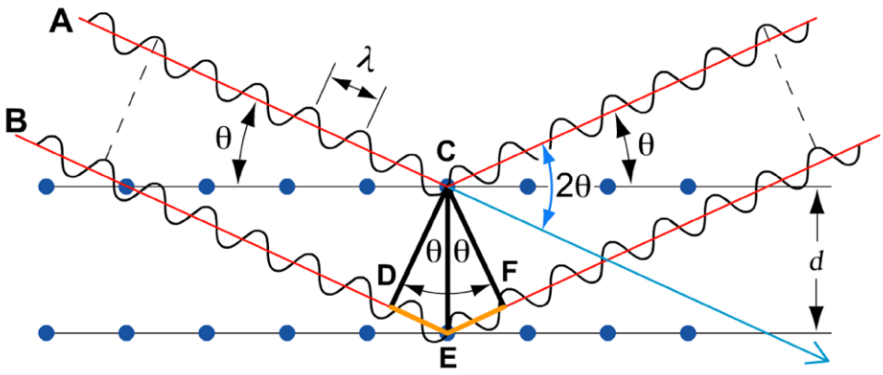

Figure 3.7 Schematic derivation for Braggs law.

In this thesis, XRD was used to determine the phases along with their crystal structures, the average grain size, and the lattice strain and parameter of the nc Cu and

Cu-1 at.% Nb samples. The used XRD device was PANalytical Empyrean Diffractometer, Fig. 3.8, with a Cu anode material (λ = 0.1542 nm). The XRD scanning range was set to be from 20º to 100º, with a step size of 0.013º and a scan rate of 0.044º s^{-1}. The operating conditions were at 45 kV, 40 mA, and 25 °C.

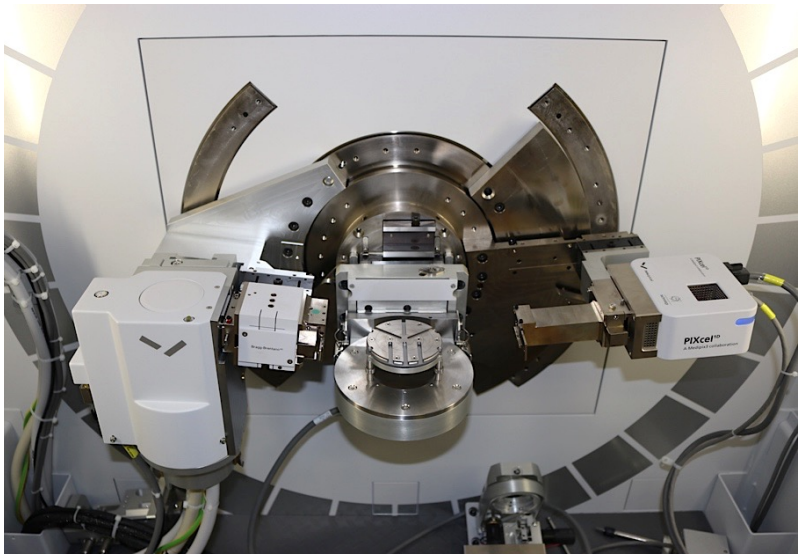

Figure 3.8 Interior view of the PANalytical Empyrean Diffractometer.

The breadth of the XRD peak gives an indication to the grain size of the sample and the lattice strain due to the milling process. Averbatch method [129] is used to precisely estimate the average grain size and lattice strain. Each single peak of all the diffraction patterns was plotted with OriginPro software and fitted with a Pseudo-Voigt function (PsdVoigt1). The Averbatch equation used in the calculations is shown in Eq. 3.2 [129]:

$$\frac{\beta^2}{tan^2\theta_o} = \frac{\lambda}{d}\left(\frac{\beta}{tan\theta_o sin\theta_o}\right) + 25\ e^2 \qquad \text{Eq. 3.2}$$

Where β is the full width at half maximum (FWHM) or the integral breadth of the peak, θ_o is the peak position (Bragg's angle), d is the average grain size, and e is

the lattice strain.

The lattice parameter of the prepared samples was calculated using a modified Cohen's method shown in Eq. 3.3 [130]

$$a = a_o + a_o k \cos^2 \theta \quad \text{Eq. 3.3}$$

Where "a" is the calculated lattice parameter for each peak, "a_o" is the average lattice parameter, and "k" is a constant.

3.2.2 Transmission Electron Microscopy (TEM)

Nowadays Transmission Electron Microscopy (TEM) is considered as an essential technique for nanomaterials characterization. TEM uses a beam of electrons that illuminates a very thin specimen in ultra-high vacuum conditions. It is capable of imaging the crystal structure along with its features like grain boundaries, dislocations, and other defects [131]. It can be used to provide information about the volume fraction distribution of the grain size [25]. The magnification power of TEM can reach to capture the finest crystal structures, such as the atoms, which is called High-Resolution TEM (HRTEM) [131]. These facts made TEM a reliable tool to validate the average grain size that was deduced from the XRD data, since TEM can really see the nc grains, unlike the XRD which can only detect the average grain size via a mathematical calculation method.

This is how TEM works, the electron beam passes through condenser lenses in order to focus it into a very thin coherent beam before striking a thin sample (~100 - 150 nm thick). The electrons that successfully passed (transmitted portion) is then focused with the help of an objective lens and translated into an image. This image passes through some electromagnetic lenses to be magnified before being received on

a fluorescent screen or, in other devices, a charge coupled device (CCD) camera [131]. The transmitted image is nothing but differences in contrast between blacks and whites, which is a translation to the variations in the amount of the material where this beam of electrons has passed (sample thickness), and variations of the electron mean free path (sample material). Heavier atoms have shorter mean free path than the lighter ones, due to the more scattering behavior in the heavy ones. There are two modes of contrast in TEM: a bright field (BF) mode, where the grains are showed in a darker color within a lighter background; and a dark field (DF) mode, which is the opposite [132].

The TEM sample preparation was carried out using double-jet electropolishing technique. For both nc Cu and nc Cu-1%Nb, a spherical sample (Fig. 3.4) was flattened using the mounting press (Fig. 3.6B) into a sheet with a thickness of ~1 mm. The sheet was then punched using a disk punch (Fig. 3.9A) into a disk of 3 mm diameter. This disk was mechanically polished using a P1200 tungsten carbide sandpaper till a thickness of ~80 μm was reached. The disk was finally electropolished at room temperature using a Fischione Automatic Twin-Jet Electropolisher (Fig. 3.9B). An electrolyte solution of Nitric acid and Ethanol was used for the electropolishing process. This process should continue till the formation of a tiny hole in the center of the sample. However, obtaining such tiny hole while keeping the surface of the sample shiny is a tricky process, since many parameters like current, voltage, and jet speed need to be controlled. Moreover, the sample needs to be removed immediately on the formation of the hole, as the thickness of the edges of the metal sample surrounding this hole should be in the nano-range to fulfill the TEM sample requirements. However, if the hole stayed for a relatively longer time (few seconds) after the hole was formed, the corrosive electrolyte will attack these thin edges. That is why this twin-jet

electropolisher is equipped with a light source at one of the jet nozzles and a photodetector at the other jet nozzle. Once the hole is created, the light passes through the hole and detected by the photocell, which in turns activate an alarm. On hearing the alarm, the operation should be immediately stopped, and the sample has to be removed out of the corrosive solution as fast as possible and gently submerged into an ethanol solution.

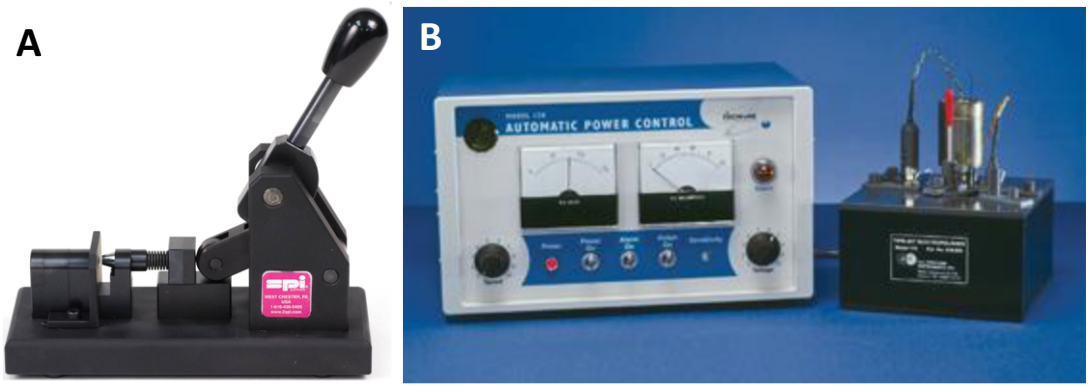

Figure 3.9 (A) 3-mm disk punch [133]. (B) Fischione Automatic Twin-Jet [134].

After preparing the samples, they were examined under an FEI Tecnai G2 TEM (Fig. 3.10). Using a voltage of 200 kV, BF and DF images were taken to determine the microstructure of the nanograins. The average grain size of 200 grains was calculated from the DF image, and a grain size distribution plot was generated. Moreover, the selected area diffraction (SAD) patterns give information about the crystal structure and the phases present, in a way similar to the XRD, but the data visualization is in the form of bright spots instead of peaks, where the spots come from the diffracted X-rays that has successfully satisfied Bragg's law. In addition, SAD patterns can give an indication of the degree of the gain refinement, where in the case of nanocrystals (larger number of grains) a high density of spots is generated to the extent that makes them form rings,

and these rings go brighter with lower grain size [135]. Furthermore, High-Resolution TEM micrograph for nc Cu-1%Nb annealed at 1073 K was performed using a JEOL-2010F TEM.

Figure 3.10 FEI Tecnai G2 TEM system.

3.2.3 Vickers Microhardness

Vickers microhardness test is a non-destructive technique that is used to evaluate a mechanical property of the materials, which is the hardness. It can also give an indication of the strength of the material through Tabor's relationship that ties between the yield strength of a material and its hardness [136], [137]. The unit of the hardness as obtained by the machine is known as Vickers Hardness number (HV),

which can be converted into pascals. In such a test, a diamond indenter with a very fine tip and a square base (pyramid-like) is applied to the surface of the sample with a specific load and for a specific time (dwell time), leaving behind a pyramid-like deformation with diagonals d1 and d2 (Fig. 3.11). These diagonals are measured precisely using the optical microscope attached to the machine. For the same load and dwell time, the smaller these diagonals are, the harder the material. The hardness value is then determined by the following equation [138]:

$$\text{H (GPa)} = \frac{1.8544 * W(gm) * 9.8 * 10^6}{(\frac{d1+d2}{2})^2 * 1000} \qquad \text{Eq. 3.3}$$

Where W is the applied weight in grams, and d1 and d2 are the diagonals of the indentation in mm.

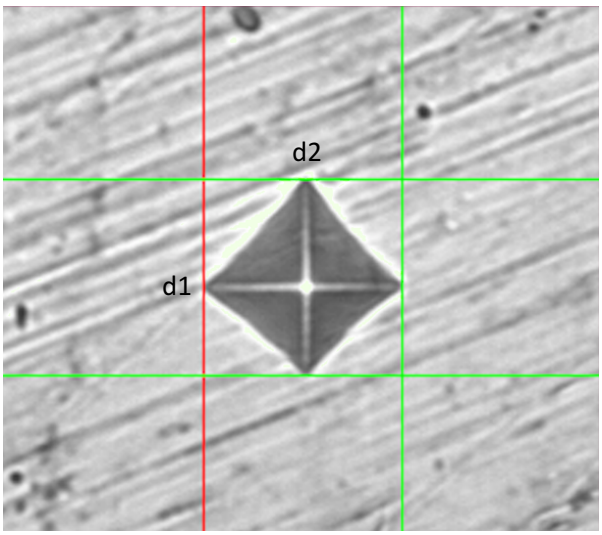

Figure 3.11 Image of the indentation showing the diagonals d1 and d2, taken by the attached optical microscope.

In this thesis, Future Tech Microhardness Tester FM-800 equipped with Fully-Automatic Hardness Testing System ARS 9000 (Fig.3.12) was used to perform the microhardness measurements, using a 25-g load for a dwell time of 10 sec. The Sample

was mounted on the steel die the same way as mentioned in section 3.1.3. At least six indentations were taken per sample in order to have the average hardness and the standard deviation.

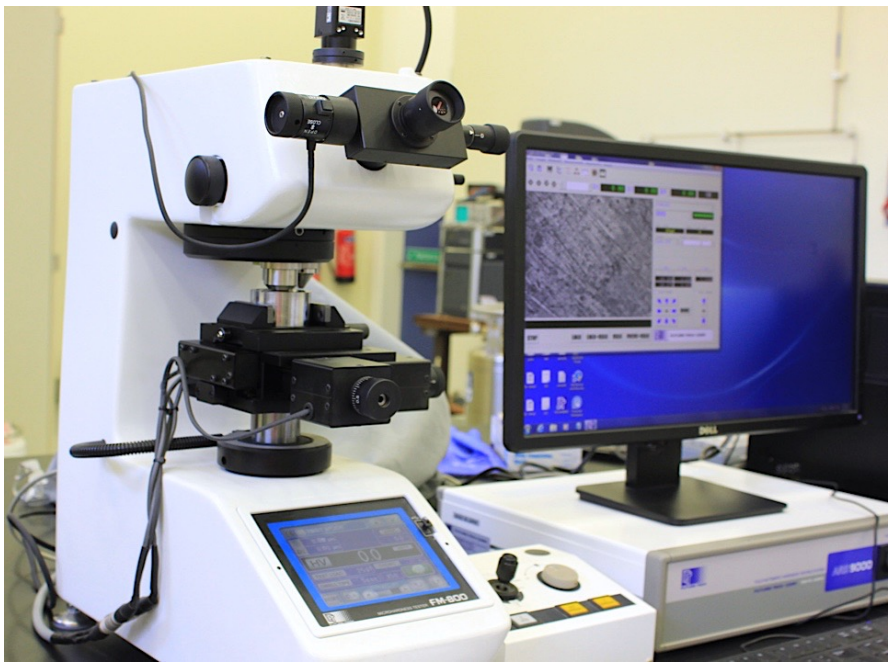

Figure 3.12 Future Tech Microhardness Tester FM-800 and Fully-Automatic Hardness Testing System ARS 9000.

3.2.4 Tensile Testing and Fracture Surface Analysis

The tensile test is considered as the most fundamental mechanical test. In this test, the specimen is put under tension till failure. The strain is detected and plotted against the applied stress, giving the stress-strain curve. Such curve provides important information about the material's properties such as; yield strength, ultimate tensile strength, uniform elongation and elongation to failure [139].

The as-milled nc Cu-1%Nb samples were punched into a dogbone-like shape with a 2-mm gauge length and a 1-mm width. The tensile specimens were mirror polished to get rid of the effects of the surface defects. The final thicknesses after

polishing were about 300-500 μm. The tensile tests were performed at ambient temperature using a strain rate of 10^{-3} s^{-1}. After performing the tensile test, the fractured pieces were collected to be analyzed under the Scanning Electron Microscopy (Hitachi S3200N SEM, Fig. 3.13) in order to investigate their ductility.

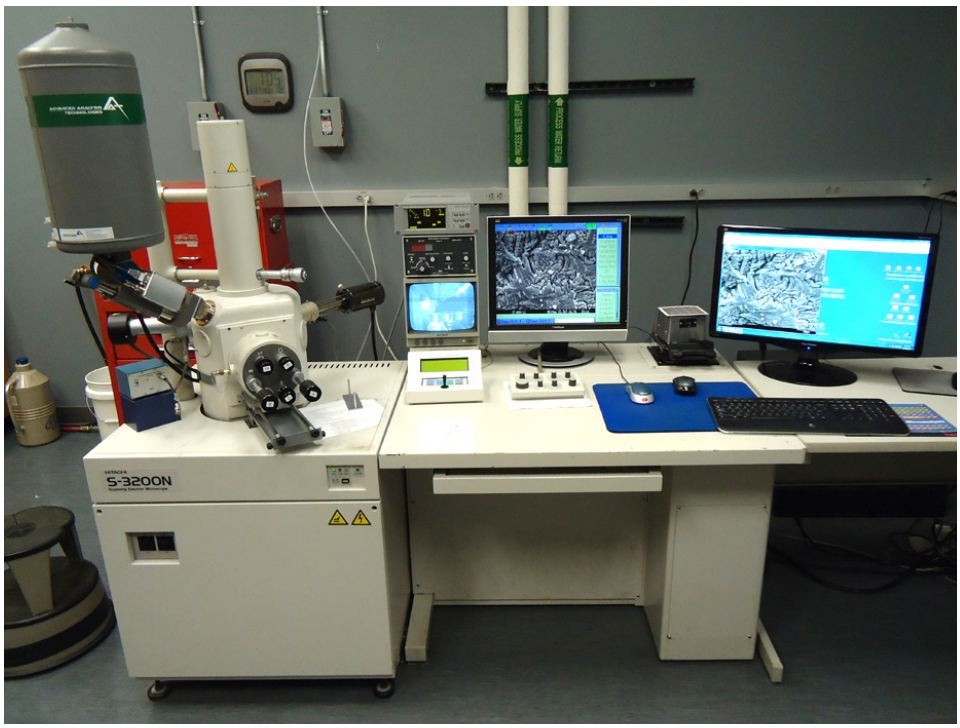

Figure 3.13 Hitachi scanning electron microscope (model S3200N) [140]

3.2.5 Four-Point Probe

The four-point probe method is a very precise technique to measure the electrical resistivity. The sample is attached to four probes/terminals which are separated by equal distances from each other as appears in Fig. 3.14. An electrical current is allowed to pass in the two outer probes while measuring the voltage between the two inner ones. The idea behind using such method is that it can measure the actual resistance of a material without being affected by the contact and lead resistances. This

advantage comes from the fact of using different electrodes for current and voltage, unlike the conventional method where the sample is connected to only two terminals [141].

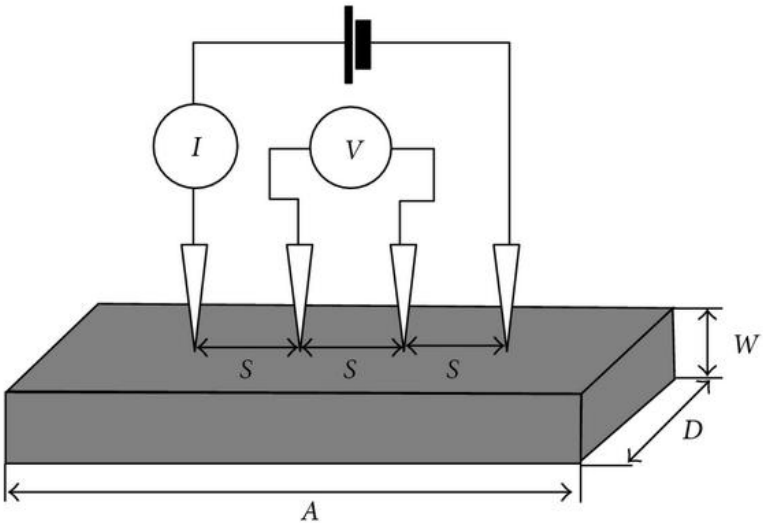

Figure 3.14 Schematic showing the way to connect a sample for measuring the electrical resistivity using a four-point probe apparatus [142].

The dc electrical resistances of the nc Cu and Cu-1%Nb were estimated using the four-point probe method at room temperature. The samples were discs with about 6 mm diameter and about 0.2 mm thickness. These disks were attached to four gold wires using a paste of conductive silver, then their electrical resistances were simply calculated through dividing the voltage by the electric current.

CHAPTER 4: RESULTS AND DISCUSSION

4.1 Evolution of Nanostructure of Cu-1 at.% Nb

Fig 4.1 shows the XRD patterns of the nc Cu-1%Nb milled for various milling hours; 1, 3, 5, 8, and 10 hr. For comparison purposes, the XRD pattern of nc Cu milled for 8 hr is also shown. The position of the peaks indicates the existence of an FCC-Cu phase. No other peaks appear for the BCC Niobium phase even after milling for only 1 hr. This confirms the success of the non-equilibrium milling (mechanical alloying) process in forming a supersaturated solid solution from the two immiscible elements, Cu and Nb. (Figure 4.2 show the Cu-Nb equilibrium phase diagram [143]). It can be noticed from Fig. 4.2 that there is very limited solid solubility of Nb in Cu at room temperature. MM/MA has been found to increase the solid solubility even for immiscible elements [80], [92]. For example, 10 at.% Nb have been reported in the work of Botcharova et al. [111] to completely dissolve into the Cu lattice after 60 hr of milling using a planetary ball mill, where there were no peaks for the elemental Nb, which agrees with our results. Furthermore, it is quite noticeable that as the milling hours increase the peaks get broader and their intensities are reduced. This is an indication of refinement in the grain size. However, to be exact sure, the integral breadth (FWHM) was obtained after fitting the peaks with a Pseudo-Voigt function (PsdVoigt1), then the averages of the grain sizes were calculated via Averbatch method [129]. The results were plotted as a function of the milling hours as shown in Fig. 4.3. It can be noticed that the grain size steeply decreased during the first five hours of milling. The grain size of the Cu-1%Nb milled for 8h is less than that of the nc Cu milled for the same period (16 vs 23 nm, respectively). This can be due to the existence of solute niobium atoms that could have reduced the ductility of the copper, embrittled

the whole mixture, and made it easier to fracture and harder to re-weld as in the case of $Al_{99}Sr_1$ [8]. This was achieved as the niobium hindered the dislocation motion inside the copper lattice. Further milling of the Cu-1%Nb caused a slight grain refinement till reaching an average grain size of 15 nm after milling for 10 hr.

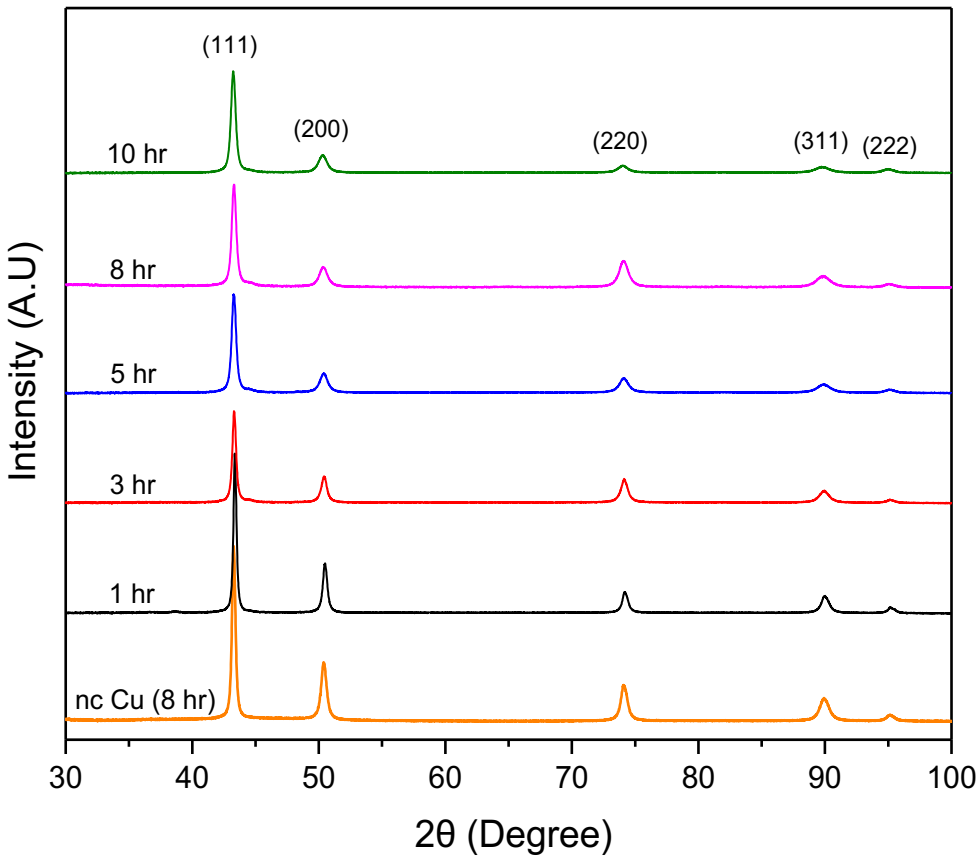

Figure 4.1 XRD patterns of nc Cu-1%Nb milled for 1, 3, 5, 8, and 10 hr compared to nc Cu (milled for 8h).

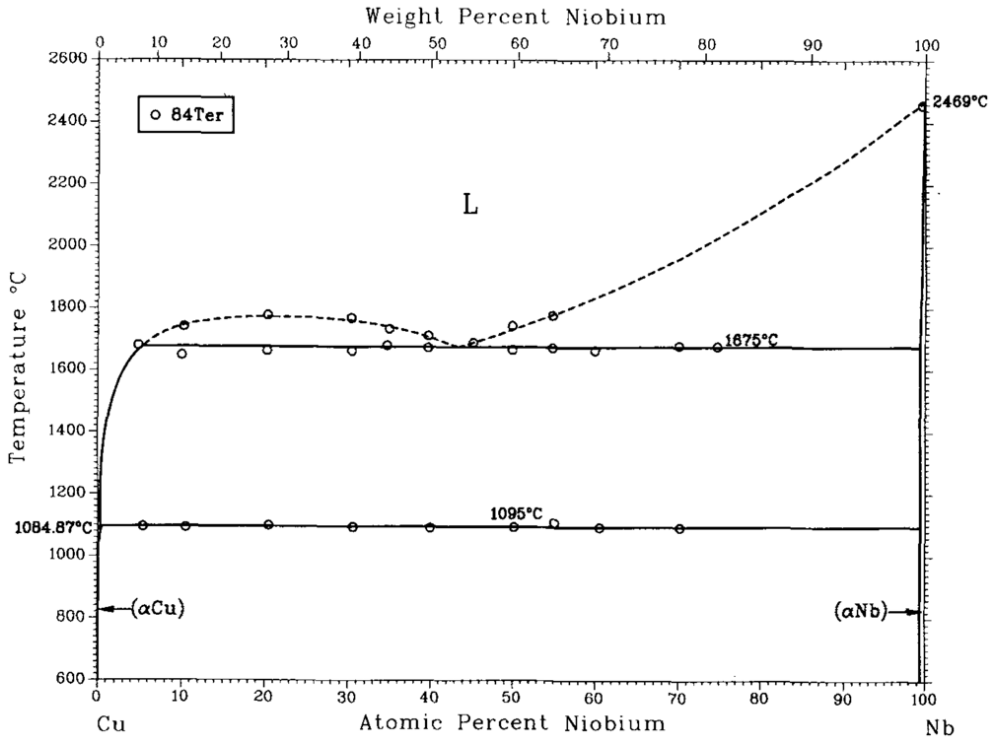

Figure 4.2 Equilibrium phase diagram of the Cu-Nb system [143].

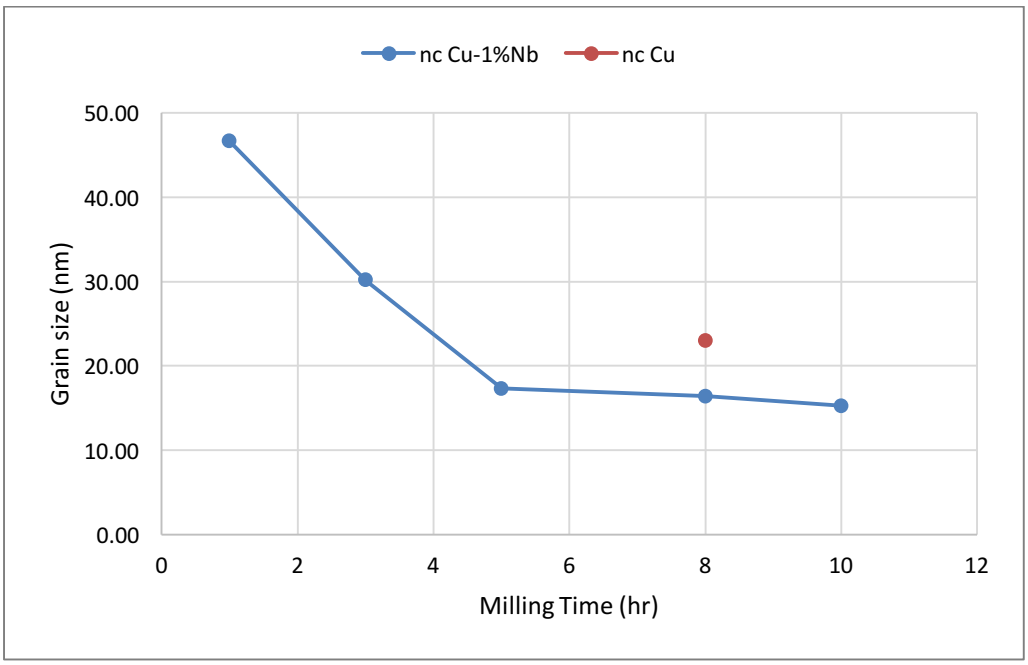

Figure 4.3 Grain size variation of nc Cu-1%Nb with milling time, compared to nc Cu milled for 8h.

Bright and dark field TEM micrographs of nc Cu and Cu-1%Nb milled for 8 hr are shown in Fig. 4.4A-D. The images show equiaxed nano grains which are randomly distributed within the structure. A statistical analysis was constructed out of several dark field images by taking the average grain size of 200 grains in each sample. The analysis revealed an average grain size of 22 and 18 nm for nc Cu and Cu-1%Nb, respectively. These data are translated in the form of statistical distributions as appears in Fig. 4.4E and F. The grain size results are in consistence with the SAD patterns, where the diffraction rings of nc Cu-1%Nb is brighter and thicker than that of nc Cu. This finding is due to the higher density of spots that came out of a higher amount of diffractions, which is an indication for a finer nanostructure in the former. It is also worth mentioning that the SAD pattern in Fig. 4.4C shows only complete rings of the FCC-Cu phase and no rings for the BCC-Nb, hence confirming the solubility of Nb in the Cu lattice, and matching with XRD results (Fig. 4.1).

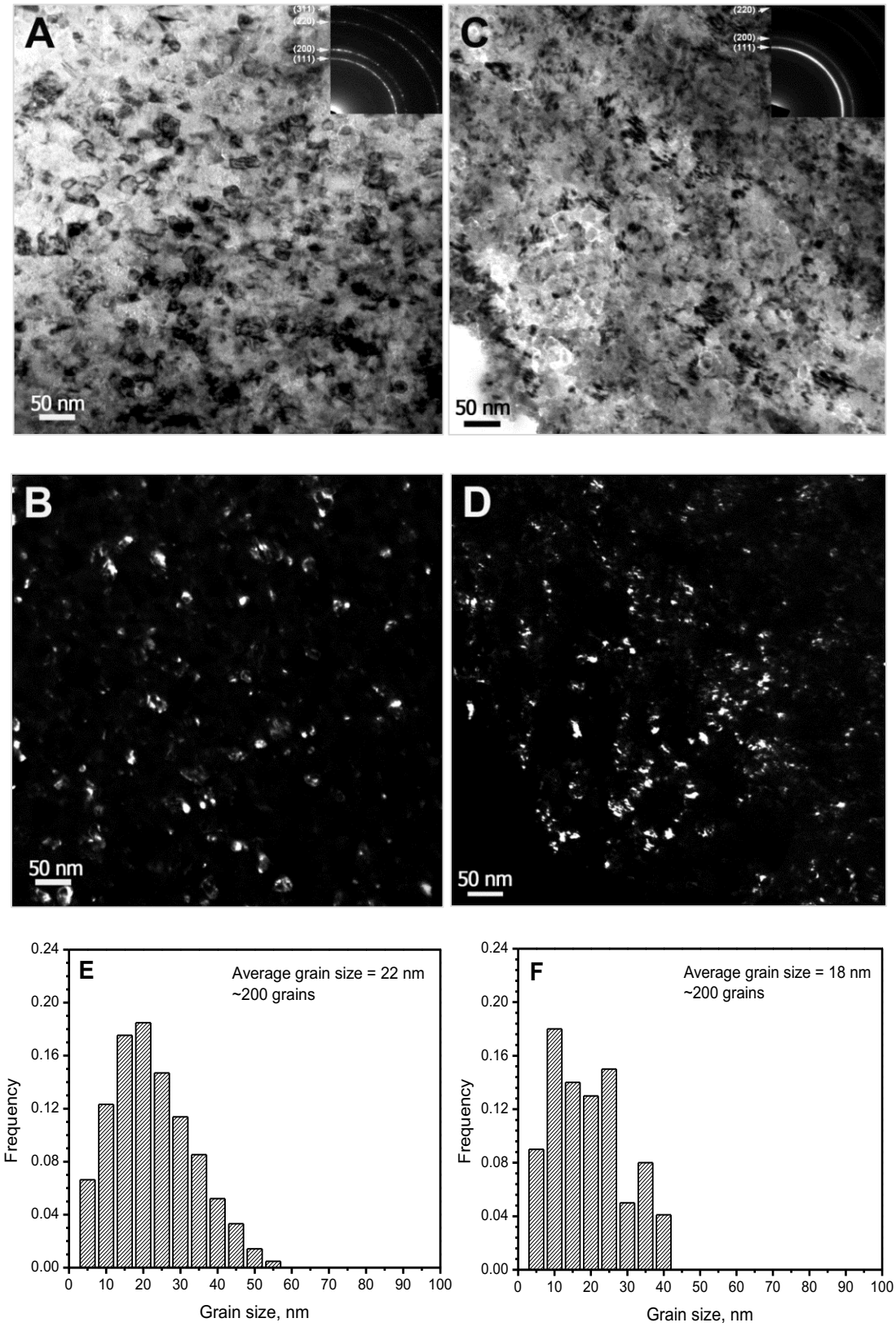

Figure 4.4 TEM observations of nc Cu and Cu-1%Nb. (A) and (B) are bright and dark-field TEM micrographs of the nc Cu, respectively. (C) and (D) are bright and dark-field TEM micrographs of the nc Cu-1%Nb, respectively. The corresponding SAD patterns are at the upper right insets of A and C. (E) and (F) are the statistical distribution plots of the grain size for the nc Cu and Cu-1%Nb, respectively.

4.2 Properties of nc Cu-1 at.% Nb

The mechanical and electrical properties including hardness, tensile strength, and electrical resistivity were measured for the as-milled nc Cu-1%Nb. These properties were compared with the nc Cu milled for 8 hr.

4.2.1 Microhardness Results

Micro-indentation test represents another way to investigate the evolution of the microstructure of a material with the milling time. Fig. 4.5 shows the values of Vickers microhardness of Cu-1 at.% Nb as a function milling time. It is clear that the hardness increased with increasing the time of milling. These results match quite well with XRD data represented in Fig. 4.2, indicating that the grain refinement is the reason behind the hardness improvement. Hence, confirming the applicability of the Hall-Petch relationship in nc materials. Such increase in hardness continued and reached a point where further milling will not have a significant improvement on the hardness. As can be seen in Fig. 4.5, there is no significant boost in the hardness of the Cu-1%Nb milled for 10 hr over that milled for 8 hr. Therefore, we believe that as for this material, milling for 8 hr is satisfyingly enough, and accordingly, we chose the Cu-1%Nb milled for 8 hr as a final product. The nc Cu-1%Nb achieved a hardness value of 3.21 GPa, which is more than that of the nc Cu (2.43 GPa). This is mainly attributed to the relatively smaller grain size of the Cu-1%Nb, the solid solution hardening mechanism, and the stresses that are induced in the material as a result of forcing the Nb atoms into the relatively tight Cu lattice.

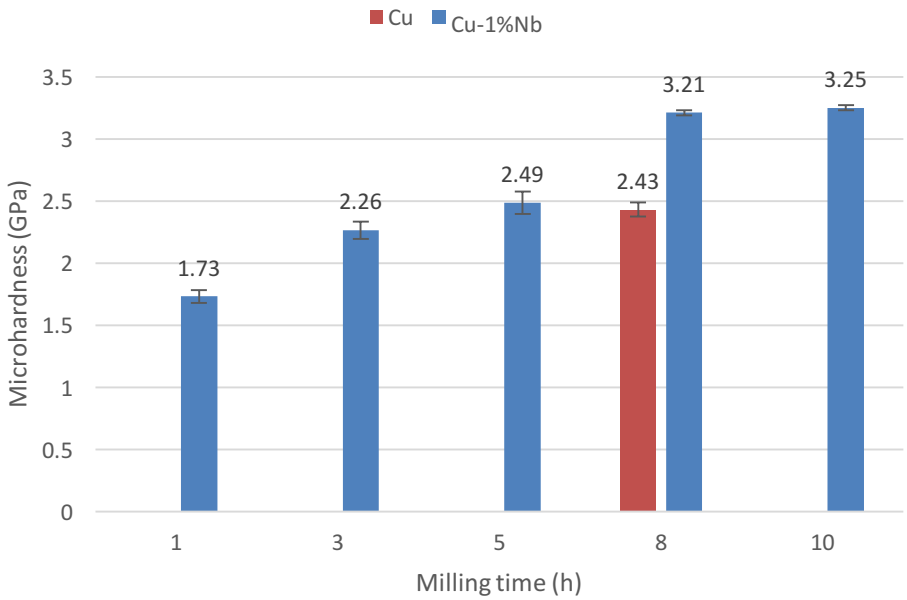

Figure 4.5 Microhardness variation of nc Cu-1%Nb with milling time, compared to nc Cu milled for 8h.

4.2.2 Tensile Test Results

Fig. 4.6 compares the tensile curve of nc Cu (prepared via in-situ cryo and room temperature milling technique by Youssef et al. [3]) to that of the Cu-1%Nb. Both tensile tests were carried out at a strain rate of 10^{-3} s^{-1} and at room-temperature. The mechanical properties for nc Cu-1%Nb exceeded those of nc Cu, where the tensile yield strength (σ_y, 0.2% offset) and the ultimate tensile strength (σ_u) of nc Cu-1%Nb are 1100 MPa and 1350 MPa, respectively compared to the 875 MPa and 1190 MPa of the nc Cu. This higher strength than that of nc Cu can be attributed to the solid solution hardening, the lattice stresses associated with supersaturation of Nb into the Cu lattice, and the relatively smaller grain size (18 nm) than that of the nc Cu (22 nm). These extraordinary ultra-high yield and ultimate tensile strengths are accompanied by decent ductility and strain hardening. nc Cu-1%Nb showed higher uniform elongation (10%) and elongation-to-failure (18%) than the nc Cu (8.5% uniform tensile elongation and

15% elongation-to-failure). It is worth mentioning that the yield strength of the nc Cu-1%Nb is more than 10X that of the conventional Cu sample (grain size ~50 μm) shown on the same figure.

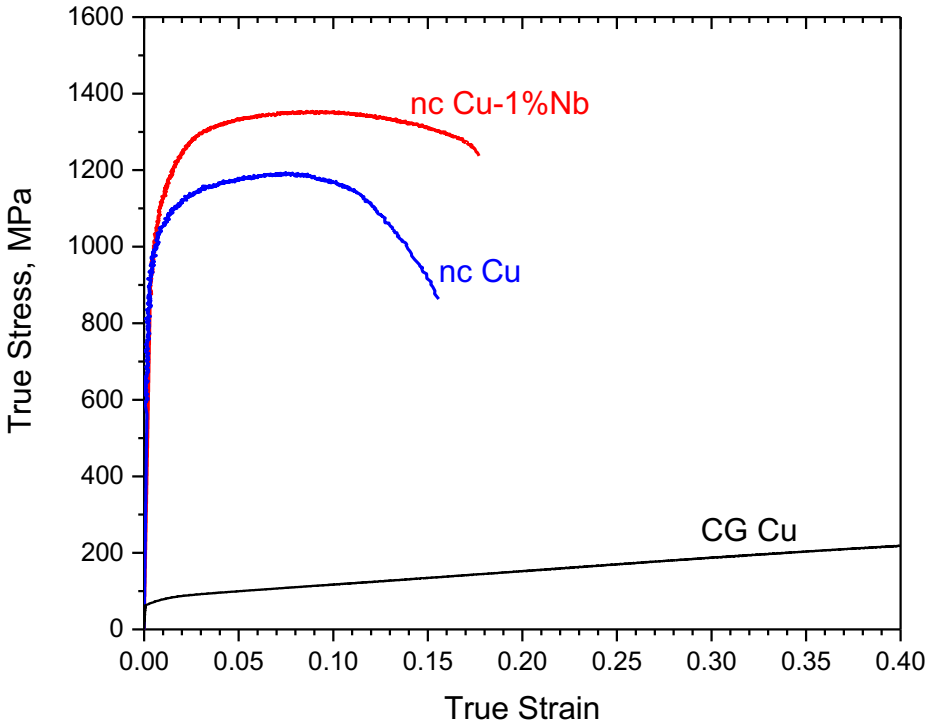

Figure 4.6 True stress-strain curves of the CG Cu in comparison to the in situ consolidated nc Cu [3], and Cu-1%Nb.

SEM Micrographs of the fracture surfaces are shown in Fig. 4.7A and B. From the morphology, it is clear that nc Cu-1%Nb (Fig. 4.7B) has more void and dimples compared to the nc Cu (Fig. 4.7A). This indicates that ductile fracture via the nucleation and coalescence of very fine sub-microvoids was more significant in the nc Cu-1%Nb sample than in the pure nc Cu. This is also consistent with the distinct enhancement in uniform elongation that is found along with noticeable strain hardening as shown from the stress-strain curves in Fig. 4.6, where the radially unstable crack growth took more time, and the stabilizing triaxial stress state was retained to higher strains.

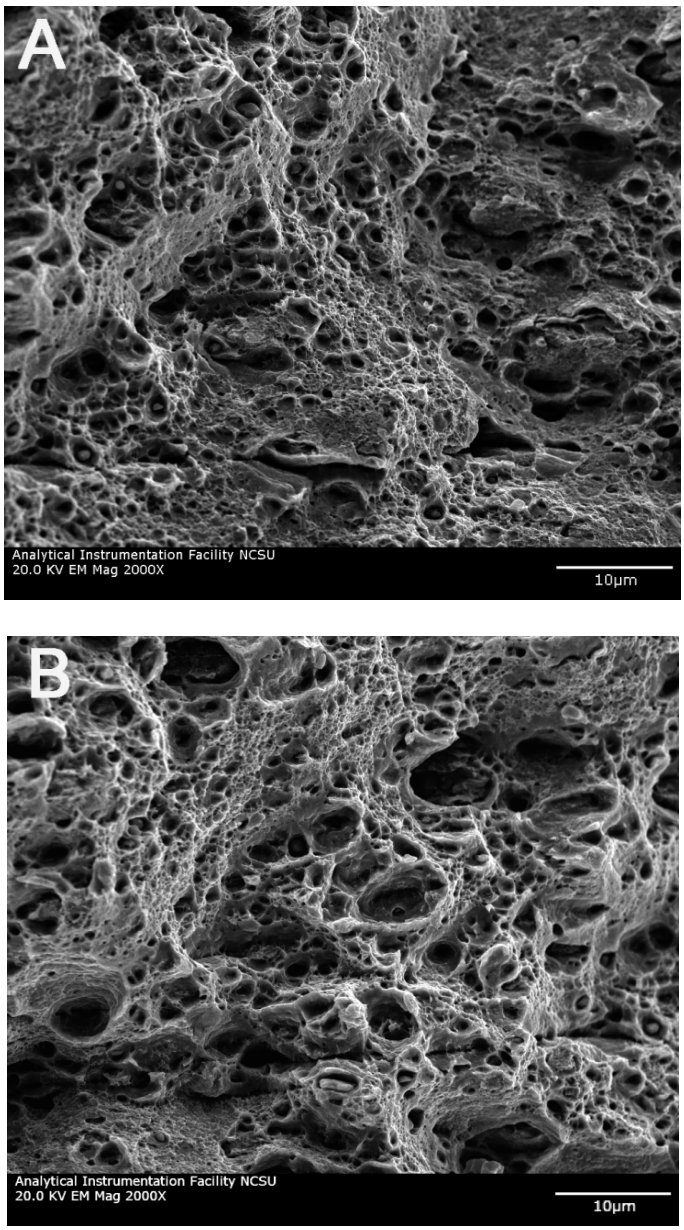

Figure 4.7 Fracture surfaces images taken by SEM after tensile testing of the as-milled (A) nc Cu, and (B) nc Cu-1%Nb.

4.2.3 Electrical Resistivity Results

Measuring the electrical resistivity for nc Cu and Cu-1%Nb at 298 K revealed values of 1.97 and 2.17 μΩ·cm, respectively. Comparing these values to the one for the CG Cu (1.78 μΩ·cm) and getting their reciprocals, we can find that the electrical conductivity of the nc Cu is about 90% of that of the CG Cu. This slight reduction in

the conductivity arises from the contributions of the grain boundaries and the dislocations. However, the addition of 1 at.% Nb to the nc Cu exhibits a minimal reduction in the electrical conductivity, as the electrical conductivity of the nc Cu-1%Nb is about 82% of that of CG Cu. Thus, the scattering of conducting electrons from the 1 at.% Nb atoms in the Cu lattice only reduces the electrical conductivity by about 8%. Such electrical conductivity is superior to that of the nc Cu-5%Nb prepared by Botcharova et al. [34], where the conductivity was significantly affected by the 5 at.% Nb as it dropped all the way to ~28% IACS. It is worth mentioning that this nc Cu-5%Nb was hot pressed at 873 K, and that the higher temperatures enhance the conductivity since it promotes the segregation of the Nb atoms outside the Cu lattice, as explained in the next section. Accordingly, the conductivity of as-milled sample should be even lower. In other words, the electric conductivity of the nc Cu-1%Nb shall be higher after annealing.

4.3 Thermal Stability of nc Cu-1 at.% Nb

This Section addresses the effect of adding one atomic percent of Niobium on the thermal stability of the nc copper. This shall be evidenced by performing structural analysis and mechanical tests on the annealed nc Cu-1 at.% Nb.

4.3.1 Structural Analysis of The Annealed Samples

As was mentioned in Chapter 2, the high temperature causes grain growth to occur in nc materials. Hence, one of the ways to check the effect of a stabilizing element on a nc material is to measure its grain size as a function of temperature and see how severe the grain growth is. This was done here by performing XRD analysis of the

annealed nc Cu-1 at.% Nb at different temperatures. Samples from the nc Cu-1%Nb milled for 8 hr were annealed at 573, 873, and 1073 K. Fig. 4.8 presents the XRD patterns for nc Cu-1 at.% Nb as-milled for 8 hr along with the annealed samples. From the figure, we can tell that the FCC structure was well preserved, and that the peaks get sharper as the broadening gradually decreased with increasing temperature. In order to determine the extent of grain growth precisely along with the strain percentage inside the lattice, analysis has been performed using the Averbatch formula as mentioned in the previous chapter (section 3.2.1), and section 4.1 in this chapter. The results have been plotted as a function of the annealing temperature, as presented in Fig. 4.9A. It can be noticed that the average grain size kept increasing with temperature till reaching 25 nm for the sample annealed at 1073 K for 1 hr. Meanwhile, the strain percentage was decreasing with increasing the annealing temperature, as the temperature has worked on reducing the strain inside the Cu lattice, indicating a partial segregation of the Nb atoms outside the lattice.

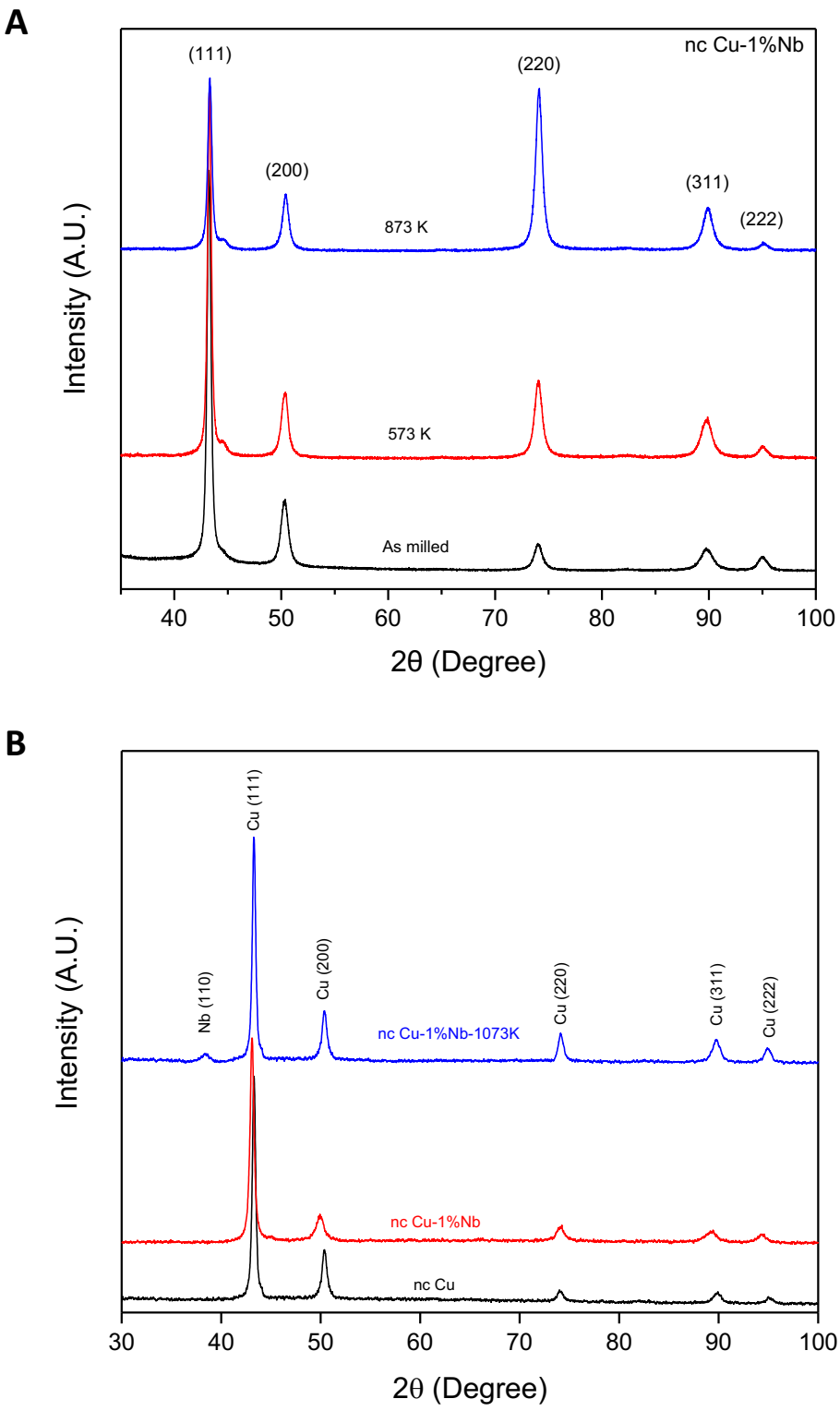

Figure 4.8 XRD patterns of (A) as-milled and annealed nc Cu-1%Nb at 573 K, 873 K. (B) as milled nc Cu and Cu-1%Nb compared to Cu-1%Nb annealed at 1073 K.

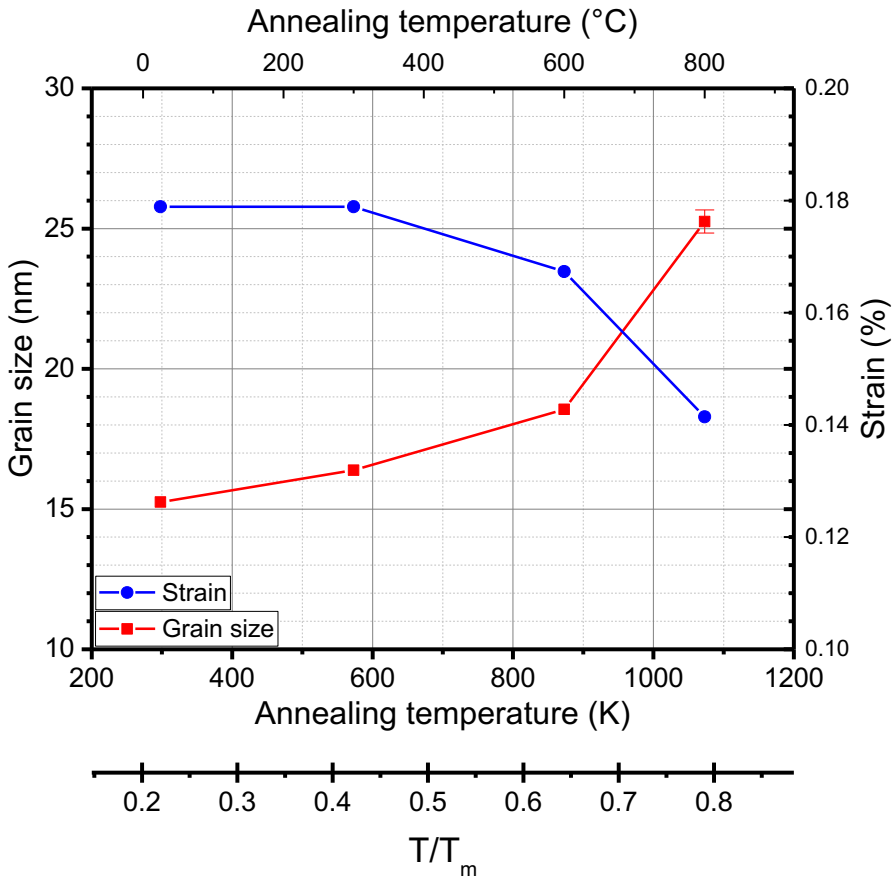

Figure 4.9 Change in grain size and stain percentage of nc Cu-1 at.%Nb with annealing temperature.

TEM observations were carried out on the annealed sample at 1073 K, as it is the highest annealing temperature where the largest grain growth may occur. Fig. 4.10A shows a BF-TEM image of nc Cu-1%Nb annealed at 1073 K for 1 hr. The figure exhibits equiaxed grains that are randomly distributed within the structure. The average grain size calculated based on 320 grains from the DF images is 45 nm (see Fig. 4.9B). It is important to note that all the grains are below 100 nm. This confirms that the crystallinity of the material is maintained in the nano-scale even after annealing at 1073K, which represents ~80% of copper's melting point. The average grain size measured with the TEM is relatively larger than that estimated using the XRD technique. However, such discrepancy in the value of the average grain size obtained

by the two techniques has been reported in many of the literature as in refs [35], [144]. Basically, TEM is considered as a more reliable technique to determine the grain size than the XRD, especially at grain size values >30 nm. As for the annealed nc Cu, its average grain size severely grew to ~3 μm, as can be seen in Fig. 4.11. Such significant grain growth is mainly due to the high GB energy of the 22-nm grain size.

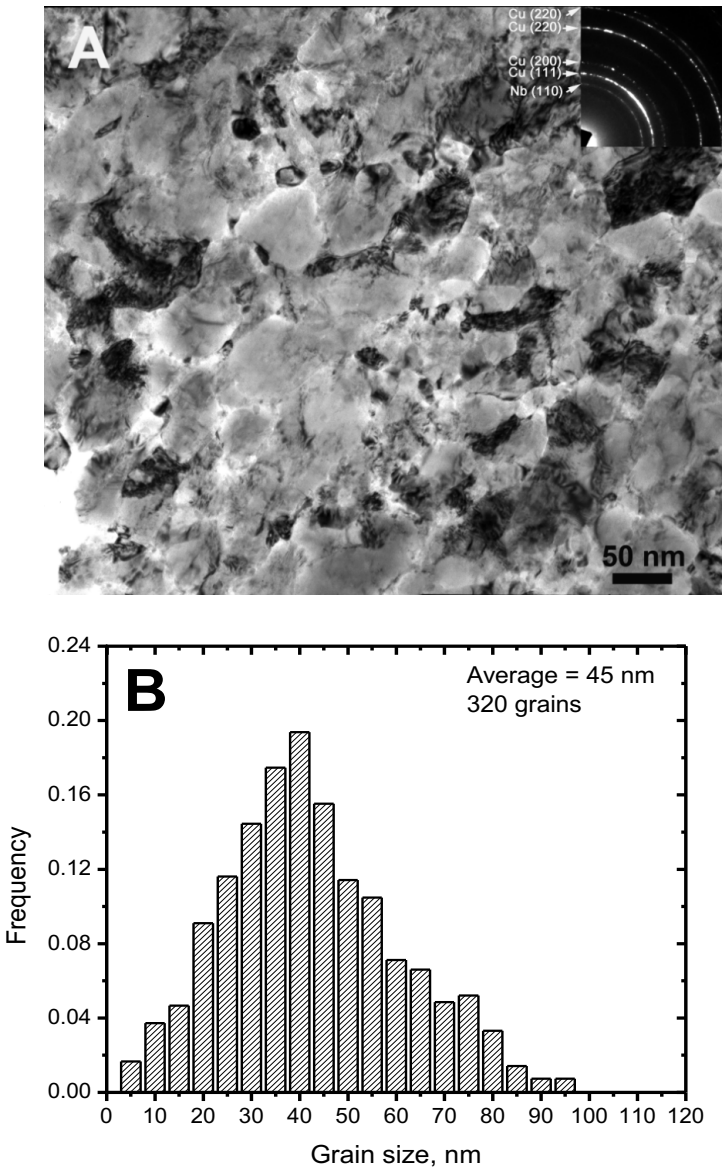

Figure 4.10 (A) BF-TEM image of nc Cu-1 at.% Nb with the SAD pattern (the inset) annealed at 800 °C (1073 K) for 1h. (B) The statistical distribution of grain size of this annealed sample.

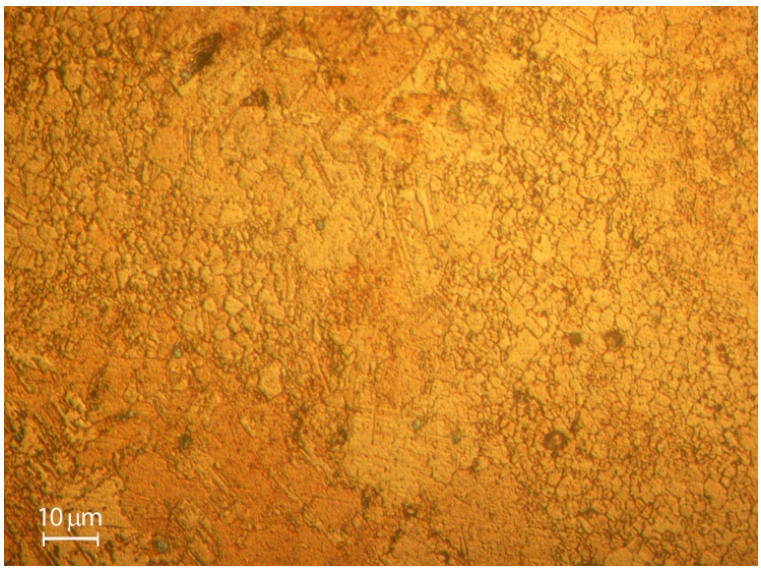

Figure 4.11 Optical microscope image showing the grains of pure nc Cu after annealing at 1073 K for 1 hr.

4.3.2 Microhardness of The Annealed Samples

Now, After we examined the effect of adding 1 at.% Nb to nc Cu on the thermal stability in terms of the grain size. Yet, there is another way to make us more confident about the results of the structural analysis by examining the practical outcomes of this effect. This shall be validated by testing the mechanical properties of the annealed samples. This section exhibits and discusses the results of the microhardness tests that were performed on the annealed nc Cu-1%Nb samples, and compares it to that of the annealed nc Cu.

Fig. 4.12 reveals the hardness variation of nanocrystalline Cu and Cu-1%Nb as a function of annealing temperature. From the Figure, with increasing the annealing temperature, the micro-hardness of the pure nc Cu significantly decreased, where it dropped to a relatively low value of 0.83 GPa after annealing at 1073 K. This agrees quite well with the result of the optical microscope image in Fig. 4.11, where the grains grew to an average of 3 µm, consequently reduces the hardness. In contrast, nc Cu-

1%Nb showed an excellent thermal stability with increasing the annealing temperature. As can be seen from Fig. 4.12, no significant decrease in the hardness of the nc Cu-1%Nb is observed up to 773 K. Meanwhile, increasing the temperature to 873 K decreased the hardness value to 3 GPa, while further annealing to 1073 K (~80% of the melting point of copper) only decreased the hardness to 2.83 GPa. This high value was achievable thanks to the 1 at.% Nb that was able to keep the grain size <100 nm. It is important to mention that the hardness value of the annealed nc Cu-1%Nb at 1074 K is still higher than the hardness of the as-milled nc Cu (2.43 GPa), regardless of having larger average grain size than that of the as-milled nc Cu (45 vs 22 nm). This is attributed to the solid solution hardening, and the existence of the relatively larger Nb atoms inside the Cu lattice, which contributes to a higher strain inside the lattice, which in turns adds on to its hardness.

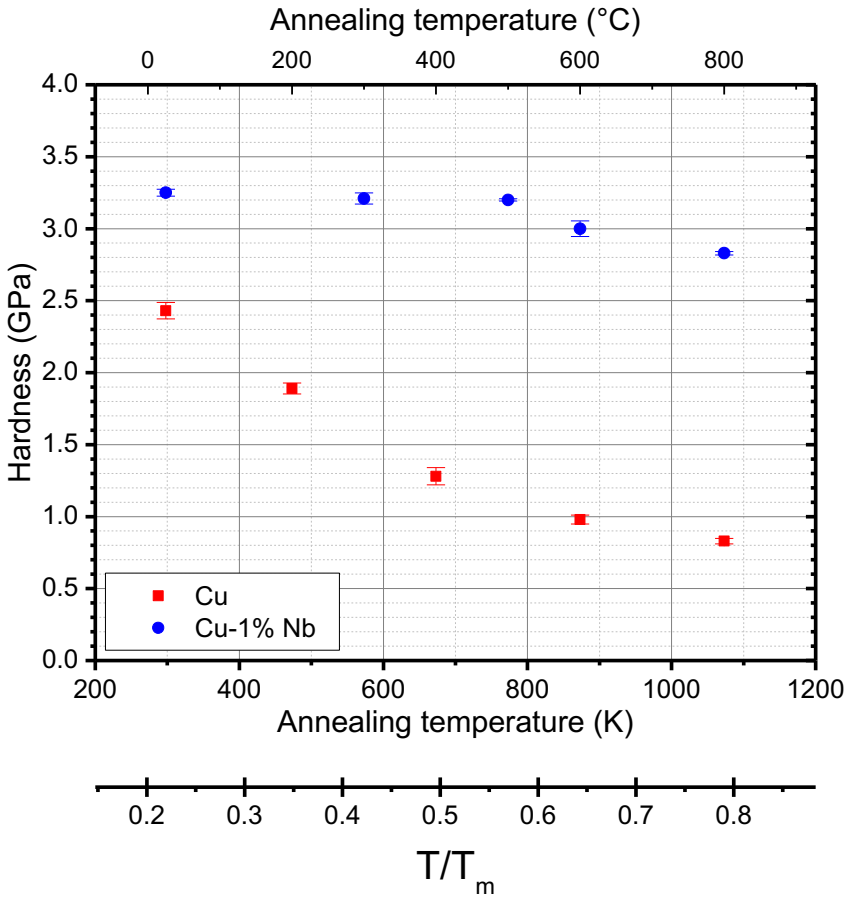

Figure 4.12 Hardness variation of the nc Cu and Cu-1 at.% Nb with the annealing temperature.

4.3.3 Mechanisms of Thermal Stability

Referring to Chapter two, there are two approaches for the stabilization mechanisms: kinetic and thermodynamic. The experimental results indicate that the main stabilizing effects are a combination of the solute drag, where the Nb atoms have pinned the grain boundaries, and the Zener pinning, where nanoparticles have precipitated out of the grains and contributed to the pinning. The non-equilibrium processing during mechanical alloying forces the larger Nb atoms to form a metastable solid solution as shown from the diffraction pattern in Fig. 4.4C. This caused the Cu lattice to have a higher strain and increased its lattice parameter from 3.6103 to 3.6193 A° as illustrated in Fig. 4.13. From the same figure, we can tell that increasing the

annealing temperature causes a reduction in the lattice parameter down to 3.6125 A°, which indicates segregation of some of the Nb atoms to the grain boundaries, releasing the stress of the lattice as well. This is also consistent with Fig. 4.9, where the strain percentage drops with increasing the annealing temperature. There are two scenarios in which segregation to grain boundaries may occur; either by the entrapment of Nb atoms at the GBs as the grains grow, or by the diffusion of Nb atoms from the lattice to the boundaries. However, the first scenario is more likely, since lattice diffusion requires higher temperatures than those where the grain growth happens in nc materials. Knauth et al. [108] used this explanation, solute entrapment by the moving boundaries as the grains grow, to account for the variations in the results of the DSC for the grain growth in nc Ni and Ni-1%Si, where the growth in nc Ni-1%Si alloy happened at a much lower rate. Similarly, we believe that solute drag is the dominant mechanism for stabilizing nc Cu at the relatively low temperatures. However, at the higher annealing temperatures, Nb atoms accumulate near the Cu grain boundaries to form nanoprecipitates. There are three pieces of evidence on such a claim: the first one is the (110) peak and ring of the BCC Nb shown in the diffraction pattern of the annealed sample at 1073 K, see Fig. 4.8 and the inset in Fig. 4.10A, respectively; the second one is the significant drop in the value of the lattice parameter of the nc Cu-1%Nb annealed at 1073 K, approaching that of nc Cu, see Fig. 4.13; the third and the strongest evidence is the High-Resolution TEM image of the nc Cu-1%Nb annealed at 1073 K (Fig. 4.14), where some precipitates of Nb (area surrounded by white dashed lines ~15 nm) can be spotted at the grain boundary of Cu. The fast Fourier transform (FFT) patterns (shown in the insets of Fig. 4.14) collected from the Nb and Cu grains (areas surrounded by yellow dashed squares) confirm the elemental composition of the selected regions.

Hence the accumulation of Nb precipitates at the grain boundaries is confirmed. Consequently, the movement of the boundary as the grain grow is impeded by the precipitation of Nb as suggested by the Zener drag effect.

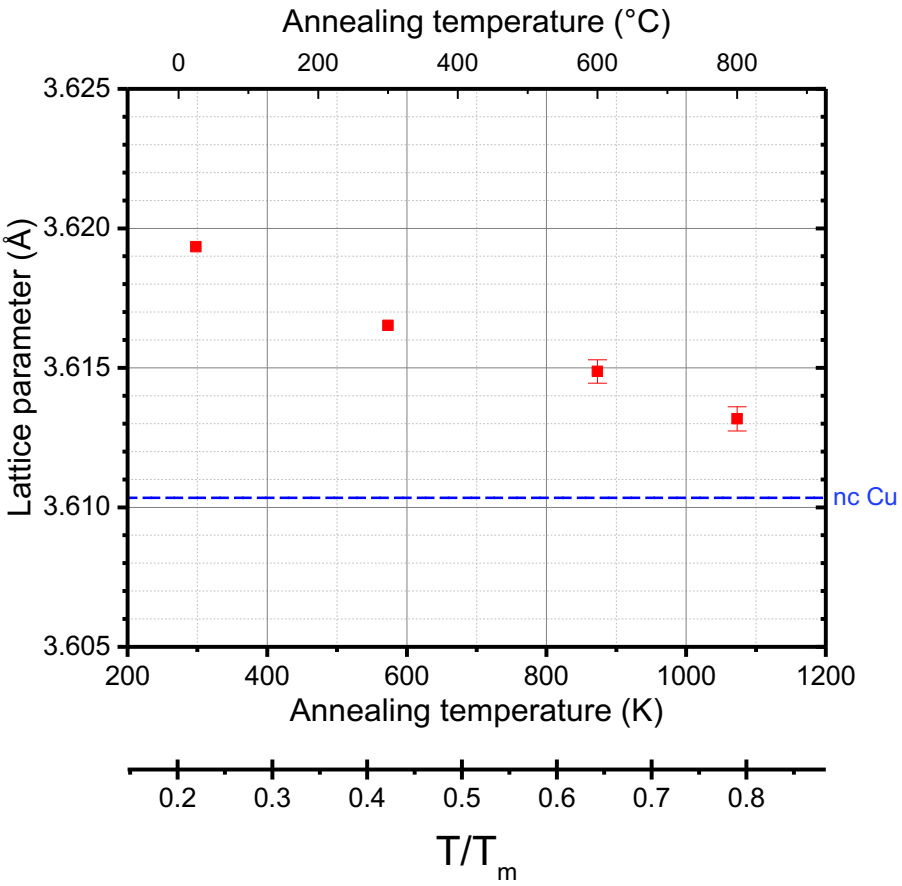

Figure 4.13 Variation in the lattice parameter of nc Cu-1%Nb with the annealing temperature.

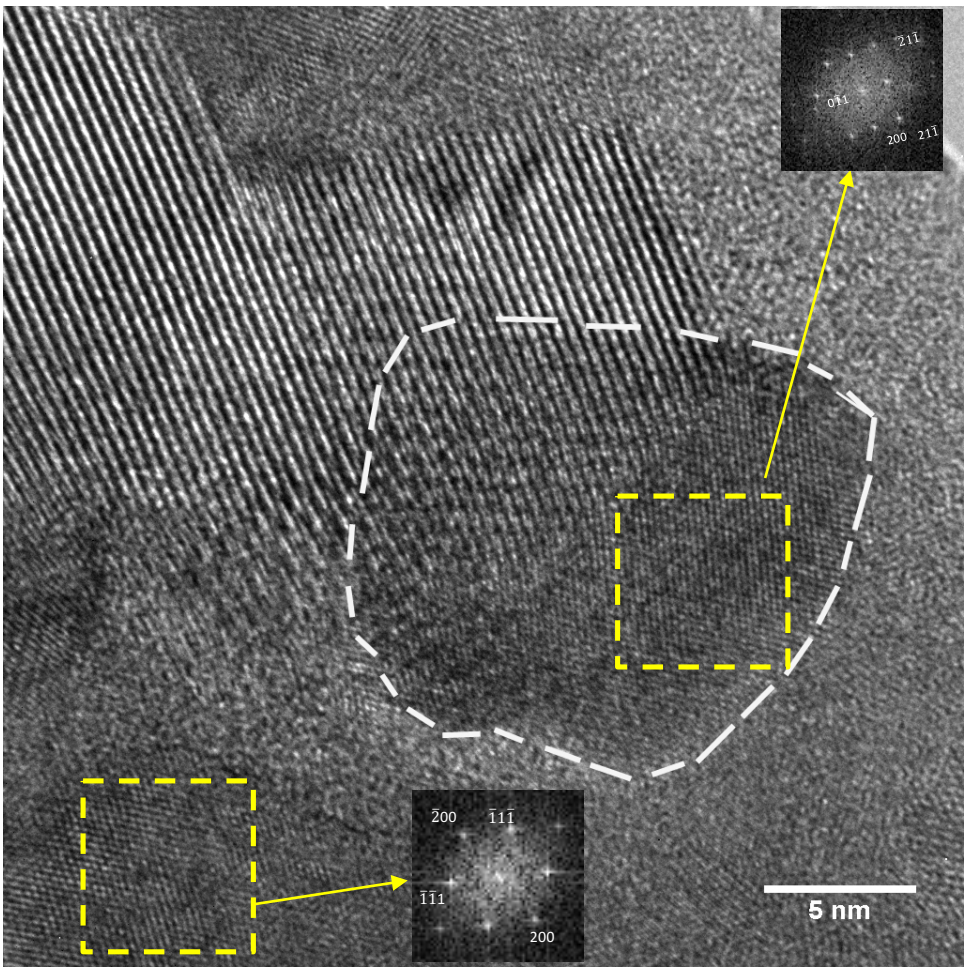

Figure 4.14 High-Resolution TEM micrograph of nc Cu-1%Nb annealed at 1073K for 1h. The top and bottom insets are the electron diffraction patterns from Nb precipitates (surrounded by white dashed lines) and Cu, respectively.

CHAPTER 5: CONCLUSIONS

Nanocrystalline Cu and Cu-1 at.% Nb samples were synthesized via mechanical alloying/milling using high-energy ball milling technique. The evolution of nanostructure and hardness in the ball milled Cu-1 at.% Nb versus milling time was examined. The tensile and the electrical properties of the nc Cu and Cu-1%Nb milled for 8 hr were inspected. In addition, their thermal stability was investigated by measuring the grain size of the samples at various annealing temperatures. The hardness of the annealed samples was measured to further support the structural investigations. The following conclusions are drawn based on the experimental findings discussed in chapter 4:

1. XRD and TEM investigations showed that the nano-crystallinity for both Cu and Cu-1%Nb was successfully achieved by ball milling technique, with average grain sizes of 22 and 18 nm, respectively.
2. The immiscible 1 at.% Nb was entirely dissolved into the Cu lattice forming a supersaturated solid solution.
3. Microhardness test carried out on the as-milled nc Cu revealed hardness value of 2.43 GPa. Meanwhile, the tensile test data showed tensile yield and ultimate strength of 875 MPa and 1190 MPa, respectively. The uniform tensile elongation and elongation-to-failure were 8.5% and 15%, respectively.
4. As-milled nc Cu-1%Nb exhibited hardness of 3.21 GPa, as well as tensile yield and ultimate strength of 1100 MPa and 1350 MPa, respectively, with uniform elongation and elongation-to-failure of 10% and 18%, respectively. Hence, nc Cu-1%Nb has superior mechanical properties compared to those of the nc Cu.
5. Adding 1 at.% Nb only reduced the electric conductivity of the pure nc Cu by 8%,

hence attained 82% IACS. Such result is considered revolutionary when compared to the 10% IACS of nc Cu with higher 10 at.% Nb content.

6. Upon annealing at 1073 K, 80% of the homologues temperature, for 1 hr, the grains of the pure nc Cu grew to an average of around 3 μm. However, the grain growth in the nc Cu-1%Nb was with an average grain size of 45 nm. Hence, indicating the effectiveness of the 1 at.% Nb in thermally stabilizing the nanostructure of the copper.
7. The lattice parameter of the as-milled nc Cu-1%Nb was relatively high (3.6193 A°). However, it started to decrease gradually after annealing till reaching 3.6125 A° at 1073 K. Which indicates the segregation of the Nb atoms out of the Cu lattice to the grain boundaries.
8. The thermal stability of nc Cu-1%Nb at lower annealing temperatures is attributed to the solute drag mechanism. Meanwhile, second phase drag mechanism is found to be the main responsible for such stability at the elevated temperature, where some precipitates accumulated at the grain boundaries as seen by HRTEM.
9. The hardness of the annealed nc Cu-1%Nb at 1073 K decreased to 2.83 GPa only. On the other side, its counterpart nc Cu has encountered a significant reduction reaching just 0.83 GPa. This also shows the effect of the 1 at.% Nb in achieving thermal stability and maintaining exceptional mechanical properties.

It is worth mentioning that the approach used to thermally stabilize the nc copper in this thesis could be applied to stabilize other nc metals and alloys. This helps to achieve remarkable high strength and hardness concurrent with good ductility and strain hardening, without sacrificing the inherent properties of the metal or the alloy, which shall open a new era for their utilization in technological applications.

REFERENCES

[1] H. Gleiter, "Nanocyrstalline Materials," *Prog. Mater. Sci.*, vol. 33, pp. 223–315, 1989.

[2] K. . S. Kumar, H. Van Swygenhoven, and S. Suresh, "Mechanical behavior of nanocrystalline metals and alloys," *Acta Mater.*, vol. 51, no. 19, pp. 5743–5774, 2003.

[3] K. M. Youssef, R. O. Scattergood, K. L. Murty, J. A. Horton, C. C. Koch, N. Carolina, J. A. Horton, and C. C. Koch, "Ultrahigh strength and high ductility of bulk nanocrystalline copper," *Appl. Phys. Lett.*, vol. 87, no. 9, pp. 1–3, 2005.

[4] C. C. Koch, K. M. Youssef, R. O. Scattergood, and K. L. Murty, "Breakthroughs in optimization of mechanical properties of nanostructured metals and alloys," *Adv. Eng. Mater.*, vol. 7, no. 9, pp. 787–794, 2005.

[5] M. A. A. Meyers, A. Mishra, and D. J. J. Benson, "Mechanical properties of nanocrystalline materials," *Prog. Mater. Sci.*, vol. 51, no. 4, pp. 427–556, 2006.

[6] K. M. Youssef, R. O. Scattergood, K. L. Murty, and C. C. Koch, "Nanocrystalline Al-Mg alloy with ultrahigh strength and good ductility," *Scr. Mater.*, vol. 54, no. 2, pp. 251–256, 2006.

[7] K. M. Youssef, Y. B. Wang, X. Z. Liao, S. N. Mathaudhu, L. J. Kecskés, Y. T. Zhu, and C. C. Koch, "High hardness in a nanocrystalline Mg97Y2Zn1 alloy," *Mater. Sci. Eng. A*, vol. 528, no. 25–26, pp. 7494–7499, 2011.

[8] S. I. Ahmed, "Thermal stabilization and mechanical properties of nanocrystalline Al and Al-Li alloys," Qatar University, 2016.

[9] F. Dalla Torre, H. Van Swygenhoven, and M. Victoria, "Nanocrystalline electrodeposited Ni: Microstructure and tensile properties," *Acta Mater.*, vol.

50, no. 15, pp. 3957–3970, 2002.

[10] C. C. Koch, “Nanostructured Materials: Processing, Properties, and Applications,” Second Edi., 2007.

[11] R. A. Matula, “Electrical resistivity of copper, gold, palladium, and silver,” *J. Phys. Chem. Ref. Data*, vol. 8, no. 4, pp. 1147–1298, 1979.

[12] P. Nath and K. L. Chopra, “Thermal conductivity of copper films,” *Thin Solid Films*, vol. 20, no. 1, pp. 53–62, 1974.

[13] G. Joseph and K. J. A. Kundig, *Copper: Its Trade, Manufacture, Use, and Environmental Status*. ASM International, 1998.

[14] S. Cheng, C. Li, F. Chai, and H. Gong, “Research on Induction Motor for Mini Electric Vehicles,” *Energy Procedia*, vol. 17, pp. 249–257, 2012.

[15] M. C. Tsai, S. W. Kang, and C. H. Lin, “A novel copper bead heat sink for computer cooling,” in *Annual IEEE Semiconductor Thermal Measurement and Management Symposium*, 2009, pp. 228–231.

[16] M. A. Abd El-Baky and M. M. Mohamed, “Heat pipe heat exchanger for heat recovery in air conditioning,” *Appl. Therm. Eng.*, vol. 27, no. 4, pp. 795–801, 2007.

[17] J. Emsley, *Nature’s building blocks : an A-Z guide to the elements*. Oxford University Press, 2001.

[18] C. Suryanarayana, “Nanocrystalline materials,” *Int. Mater. Rev.*, vol. 40, no. 2, pp. 41–64, 1995.

[19] C. Suryanarayana and C. C. Koch, “Nanocrystalline materials - Current research and future directions,” *Hyperfine Interact.*, vol. 130, no. 1–4, pp. 5–44, 2000.

[20] F. Liu and R. Kirchheim, “Grain boundary saturation and grain growth,” *Scr. Mater.*, vol. 51, no. 6, pp. 521–525, 2004.

[21] M. T. Marques, V. Livramento, J. B. Correia, A. Almeida, and R. Vilar, “Production of copper-niobium carbide nanocomposite powders via mechanical alloying,” *Mater. Sci. Eng. A*, vol. 399, no. 1–2, pp. 382–386, 2005.

[22] K. A. Darling, R. N. Chan, P. Z. Wong, J. E. Semones, R. O. Scattergood, and C. C. Koch, “Grain-size stabilization in nanocrystalline FeZr alloys,” *Scr. Mater.*, vol. 59, no. 5, pp. 530–533, 2008.

[23] T. Frolov, K. A. Darling, L. J. Kecskés, and Y. Mishin, “Stabilization and strengthening of nanocrystalline copper by alloying with tantalum,” *Acta Mater.*, vol. 60, no. 5, pp. 2158–2168, 2012.

[24] K. A. Darling, A. J. Roberts, Y. Mishin, S. N. Mathaudhu, and L. J. Kecskés, “Grain size stabilization of nanocrystalline copper at high temperatures by alloying with tantalum,” *J. Alloys Compd.*, vol. 573, pp. 142–150, 2013.

[25] M. Saber, “Thermal Stability of Nanocrystalline Alloys by Solute Additions and A Thermodynamic Modeling,” Raleigh, North Carolina, 2013, pp. 1–200.

[26] M. A. Atwater, R. O. Scattergood, and C. C. Koch, “The stabilization of nanocrystalline copper by zirconium,” *Mater. Sci. Eng. A*, vol. 559, pp. 250–256, 2013.

[27] A. Khalajhedayati and T. J. Rupert, “High-Temperature Stability and Grain Boundary Complexion Formation in a Nanocrystalline Cu-Zr Alloy,” *Jom*, vol. 67, no. 12, pp. 2788–2801, 2015.

[28] C. C. Koch, R. O. Scattergood, K. A. Darling, and J. E. Semones,

"Stabilization of nanocrystalline grain sizes by solute additions," *J. Mater. Sci.*, vol. 43, no. 23–24, pp. 7264–7272, 2008.

[29] F. R. de Boer, R. Boom, W. C. M. Mattens, A. R. Miedema, and A. K. Niessen, "Cohesion in Metals: Transition Metal Alloys," *Cohesion and Structure*, no. 1. p. 758, 1989.

[30] M. D. Abad, S. Parker, D. Kiener, M. M. Primorac, and P. Hosemann, "Microstructure and mechanical properties of CuxNb1-x alloys prepared by ball milling and high pressure torsion compacting," *J. Alloys Compd.*, vol. 630, pp. 117–125, 2015.

[31] E. Botcharova, M. Heilmaier, J. Freudenberger, G. Drew, D. Kudashow, U. Martin, and L. Schultz, "Supersaturated solid solution of niobium in copper by mechanical alloying," *J. Alloys Compd.*, vol. 351, no. 1–2, pp. 119–125, 2003.

[32] E. Botcharova, J. Freudenberger, and L. Schultz, "Cu-Nb alloys prepared by mechanical alloying and subsequent heat treatment," *J. Alloys Compd.*, vol. 365, no. 1–2, pp. 157–163, 2004.

[33] E. Botcharova, J. Freudenberger, A. Gaganov, K. Khlopkov, and L. Schultz, "Novel Cu-Nb-wires: Processing and characterisation," *Mater. Sci. Eng. A*, vol. 416, no. 1–2, pp. 261–268, 2006.

[34] E. Botcharova, J. Freudenberger, and L. Schultz, "Mechanical and electrical properties of mechanically alloyed nanocrystalline Cu-Nb alloys," *Acta Mater.*, vol. 54, no. 12, pp. 3333–3341, 2006.

[35] R. shan Lei, M. p. Wang, M. xing Guo, Z. Li, and Q. y. Dong, "Microstructure evolution and thermal stability of nanocrystalline Cu-Nb alloys during heat treatment," *Trans. Nonferrous Met. Soc. China (English Ed.*, vol. 19, no. 2, pp.

272–276, 2009.

[36] R. S. Lei, M. P. Wang, Z. Li, H. G. Wei, W. C. Yang, Y. L. Jia, and S. Gong, "Structure evolution and solid solubility extension of copper-niobium powders during mechanical alloying," *Mater. Sci. Eng. A*, vol. 528, no. 13–14, pp. 4475–4481, 2011.

[37] R. Lei, S. Xu, M. Wang, and H. Wang, "Microstructure and properties of nanocrystalline copper-niobium alloy with high strength and high conductivity," *Mater. Sci. Eng. A*, vol. 586, pp. 367–373, 2013.

[38] R. Lei, M. Wang, S. Xu, H. Wang, and G. Chen, "Microstructure, Hardness Evolution, and Thermal Stability Mechanism of Mechanical Alloyed Cu-Nb Alloy during Heat Treatment," *Metals (Basel).*, vol. 6, no. 9, p. 194, 2016.

[39] S. Mula, H. Bahmanpour, S. Mal, P. C. Kang, M. Atwater, W. Jian, R. O. Scattergood, and C. C. Koch, "Thermodynamic feasibility of solid solubility extension of Nb in Cu and their thermal stability," *Mater. Sci. Eng. A*, vol. 539, pp. 330–336, 2012.

[40] C. Suryanarayana, "Structure and properties of nanocrystalline materials," *Bull. Mater. Sci*, vol. 17, no. 4, pp. 307–346, 1994.

[41] A. A. Balandin, "Thermal properties of graphene and nanostructured carbon materials.," *Nat. Mater.*, vol. 10, no. 8, p. 569, 2011.

[42] S. K. Panda, A. Antonakos, E. Liarokapis, S. Bhattacharya, and S. Chaudhuri, "Optical properties of nanocrystalline SnS2 thin films," *Mater. Res. Bull.*, vol. 42, no. 3, pp. 576–583, 2007.

[43] A. Hernando, "Magnetic properties and spin disorder in nanocrystalline materials," *J. Phys. Condens. Matter*, vol. 11, no. 48, pp. 9455–9482, 1999.

[44] G. Herzer, “Nanocrystalline soft magnetic materials,” *J. Magn. Magn. Mater.*, vol. 157–158, pp. 133–136, 1996.

[45] K. J. H. M.Legros, B. R. Elliott, M.N.Rittner, J.R.Weertman, “Microsample tensile testing of nanocrystalline metals,” *Philos. Mag.*, vol. 80, no. 4, pp. 1017–1026, 2000.

[46] H. Gleiter, “Nanocrystalline Materials,” *Prog. Mater. Sci.*, vol. 33, no. 4, pp. 223–315, 1989.

[47] M. Cherkaoui and L. Capolungo, “Atomistic and Continuum Modeling of Nanocrystalline Materials,” *Springer Ser. Mater. Sci.*, vol. 112, pp. 1–27, 2009.

[48] H. Gleiter, “Nanostructured materials: basic concepts and microstructure,” *Acta Mater.*, vol. 48, no. 1, pp. 1–29, 2000.

[49] Y. Wang, M. Chen, F. Zhou, and E. Ma, “High tensile ductility in a nanostructured metal,” *Nature*, vol. 419, no. 31 October, pp. 912–914, 2002.

[50] L. Lu, Y. Shen, X. Chen, L. Qian, and K. Lu, “Ultrahigh strength and high electrical conductivity in copper.,” *Science*, vol. 304, no. 5669, pp. 422–6, 2004.

[51] E. Ma, “Four Approaches to Improve the Tensile Ductility of High-Strength Nanocrystalline Metals,” *J. Mater. Eng. Perform.*, vol. 14, no. August, pp. 430–434, 2005.

[52] S. Cheng, E. Ma, Y. M. Wang, L. J. Kecskés, K. M. Youssef, C. C. Koch, U. P. Trociewitz, and K. Han, “Tensile properties of in situ consolidated nanocrystalline Cu,” *Acta Mater.*, vol. 53, no. 5, pp. 1521–1533, 2005.

[53] L. Lu, X. Chen, X. Huang, and K. Lu, “Revealing the Maximum Strength,” *Science (80-.).*, vol. 323, no. January, pp. 2007–2010, 2009.

[54] Y. Wang, M. Chen, F. Zhou, and E. Ma, “High tensile ductility in a nanostructured metal.,” *Nature*, vol. 419, no. 6910, pp. 912–915, 2002.

[55] Y. M. Wang, K. Wang, D. Pan, K. Lu, K. J. Hemker, and E. Ma, “Microsample tensile testing of nanocrystalline copper,” *Scr. Mater.*, vol. 48, no. 12, pp. 1581–1586, 2003.

[56] Q. Wei, D. Jia, K. T. Ramesh, and E. Ma, “Evolution and microstructure of shear bands in nanostructured Fe,” *Appl. Phys. Lett.*, vol. 81, no. 7, pp. 1240–1242, 2002.

[57] T. R. Malow and C. C. Koch, “Mechanical properties in tension of mechanically attrited nanocrystalline iron by the use of the miniaturized disk bend test,” *Acta Mater.*, vol. 46, no. 18, pp. 6459–6473, 1998.

[58] W. P. K. Sezer OZerinc, a Kaiping Tai, Nhon Q. Vo, Pascal Bellon, Robert S. Averbackb, “Grain boundary doping strengthens nanocrystalline copper alloys,” *Scr. Mater.*, vol. 67, no. 7–8, pp. 720–723, 2012.

[59] A. Godon, J. Creus, S. Cohendoz, E. Conforto, X. Feaugas, P. Girault, and C. Savall, “Effects of grain orientation on the Hall-Petch relationship in electrodeposited nickel with nanocrystalline grains,” *Scr. Mater.*, vol. 62, no. 6, pp. 403–406, 2010.

[60] H. Kotan, K. A. Darling, M. Saber, C. C. Koch, and R. O. Scattergood, “Effect of zirconium on grain growth and mechanical properties of a ball-milled nanocrystalline FeNi alloy,” *J. Alloys Compd.*, vol. 551, pp. 621–629, 2013.

[61] V. M. S. Muthaiah and S. Mula, “Effect of zirconium on thermal stability of nanocrystalline aluminium alloy prepared by mechanical alloying,” *J. Alloys Compd.*, vol. 688, pp. 571–580, 2016.

[62] M. Rajabi, R. M. Sedighi, and S. M. Rabiee, “Thermal stability of nanocrystalline Mg-based alloys prepared via mechanical alloying,” *Trans. Nonferrous Met. Soc. China*, vol. 26, no. 2, pp. 398–405, 2016.

[63] W. Callister and D. Rethwisch, *Materials science and engineering: an introduction*, vol. 94. 2007.

[64] H. G. A.H. Chokshi, A. Rosen, J. Karch, “On the validity of the hall-petch relationship in nanocrystalline materials,” vol. 23, no. c, 1989.

[65] C. C. Koch, R. O. Scattergood, and K. L. Murty, “The mechanical behavior of multiphase nanocrystalline materials,” *Jom*, vol. 59, no. 3, pp. 66–70, 2007.

[66] R. O. Scattergood, C. C. Koch, K. L. Murty, and D. Brenner, “Strengthening mechanisms in nanocrystalline alloys,” *Mater. Sci. Eng. A*, vol. 493, no. 1–2, pp. 3–11, 2008.

[67] T. J. Rupert, J. C. Trenkle, and C. A. Schuh, “Enhanced solid solution effects on the strength of nanocrystalline alloys,” *Acta Mater.*, vol. 59, no. 4, pp. 1619–1631, 2011.

[68] T. J. Rupert, “Solid solution strengthening and softening due to collective nanocrystalline deformation physics,” *Scr. Mater.*, vol. 81, no. Md, pp. 44–47, 2014.

[69] R. V. Koteswararao and C. C. Koch, *Nanocrystalline Materials: Mechanical Properties*, no. December. Elsevier Ltd., 2016.

[70] R. Labusch, “A Statistical Theory of Solid Solution Hardening,” *Phys. status solidi*, vol. 41, no. 2, pp. 659–669, 1970.

[71] M. S. El-Eskandarany, “Ball milling as a powerful nanotechnological tool for fabrication of nanomaterials,” *Mech. Alloy. Nanotechnology, Mater. Sci.*

Powder Metall., pp. 84–112, 2015.

[72] T. Björk, M. Berger, R. Westergård, S. Hogmark, and J. Bergström, "New physical vapour deposition coatings applied to extrusion dies," *Surf. Coatings Technol.*, vol. 146–147, pp. 33–41, 2001.

[73] S. Vallejos, F. Di Maggio, T. Shujah, and C. Blackman, "Chemical Vapour Deposition of Gas Sensitive Metal Oxides," *Chemosensors*, vol. 4, no. 1, p. 4, 2016.

[74] H. L. Porter, C. Mion, A. L. Cai, X. Zhang, and J. F. Muth, "Growth of ZnO films on C-plane (0 0 0 1) sapphire by pulsed electron deposition (PED)," *Mater. Sci. Eng. B Solid-State Mater. Adv. Technol.*, vol. 119, no. 2, pp. 210–212, 2005.

[75] M. B. Ward, R. Brydson, and R. F. Cochrane, "Mn nanoparticles produced by inert gas condensation," *J. Phys. Conf. Ser.*, vol. 26, pp. 296–299, 2006.

[76] V. An and B. Liu, "Synthesis of multilevel ZnS/ZnO nanostructures by electrospark erosion," vol. 12, no. 12, pp. 639–644, 2015.

[77] Y. Yang, K.-H. Kim, and J. L. Ong, "A review on calcium phosphate coatings produced using a sputtering process--an alternative to plasma spraying.," *Biomaterials*, vol. 26, no. 3, pp. 327–337, 2005.

[78] W. Z. and K. M. Krishnan, "Epitaxial patterning of thin-films: conventional lithographies and beyond," *J. Micromechanics Microengineering*, vol. 24, no. 9, p. 93001, 2014.

[79] A. Dhawan, Y. Du, D. Batchelor, H. N. Wang, D. Leonard, V. Misra, M. Ozturk, M. D. Gerhold, and T. Vo-Dinh, "Hybrid top-down and bottom-up fabrication approach for wafer-scale plasmonic nanoplatforms," *Small*, vol. 7,

no. 6, pp. 727–731, 2011.

[80] C. Suryanarayana, “Mechanical Alloying and Milling,” *Key Eng. Mater.*, vol. 103, no. 1–2, pp. 1–184, 2001.

[81] J. M. Tao, X. K. Zhu, R. O. Scattergood, and C. C. Koch, “The thermal stability of high-energy ball-milled nanostructured Cu,” *Mater. Des.*, vol. 50, pp. 22–26, 2013.

[82] D. Roy, M. A. Atwater, K. M. Youssef, J. C. Ledford, R. O. Scattergood, and C. C. Koch, “Studies on thermal stability, mechanical and electrical properties of nano crystalline Cu99.5Zr0.5 alloy,” *J. Alloys Compd.*, vol. 558, pp. 44–49, 2013.

[83] Y. Champion, C. Langlois, S. Guérin-Mailly, P. Langlois, J.-L. Bonnentien, and M. J. Hytch, “Near-perfect elastoplasticity in pure nanocrystalline copper.,” *Science*, vol. 300, no. 5617, pp. 310–311, 2003.

[84] W. Cao, “High energy ball milling process for nanomaterial synthesis.” [Online]. Available: http://www.understandingnano.com/nanomaterial-synthesis-ball-milling.html. [Accessed: 01-Oct-2016].

[85] C. C. Koch and J. D. Whittenberger, “Mechanical milling/alloying of intermetallics,” *Intermetallics*, vol. 4, no. 5, pp. 339–355, 1996.

[86] C. H. Moelle and H. J. Fecht, “Thermal stability of nanocrystalline iron prepared by mechanical attrition,” *Nanostructured Mater.*, vol. 6, no. 1–4, pp. 421–424, 1995.

[87] R. Gupta, R. K. Singh Raman, and C. C. Koch, “Grain growth behaviour and consolidation of ball-milled nanocrystalline Fe-10Cr alloy,” *Mater. Sci. Eng. A*, vol. 494, no. 1–2, pp. 253–256, 2008.

[88] R. K. Guduru, K. L. Murty, K. M. Youssef, R. O. Scattergood, and C. C. Koch, "Mechanical behavior of nanocrystalline copper," *Mater. Sci. Eng. A*, vol. 463, no. 1–2, pp. 14–21, 2007.

[89] S. Mula, D. Setman, K. M. Youssef, R. O. Scattergood, and C. C. Koch, "Structural evolution of Cu(1−X)YX alloys prepared by mechanical alloying: Their thermal stability and mechanical properties," *J. Alloys Compd.*, vol. 627, pp. 108–116, 2015.

[90] F. Zhou, X. Z. Liao, Y. T. Zhu, S. Dallek, and E. J. Lavernia, "Microstructural evolution during recovery and recrystallization of a nanocrystalline Al-Mg alloy prepared by cryogenic ball milling," *Acta Mater.*, vol. 51, no. 10, pp. 2777–2791, 2003.

[91] L. Shaw, H. Luo, J. Villegas, and D. Miracle, "Thermal stability of nanostructured Al93Fe3Cr2Ti2 alloys prepared via mechanical alloying," *Acta Mater.*, vol. 51, no. 9, pp. 2647–2663, 2003.

[92] P. C. Millett, R. P. Selvam, and A. Saxena, "Stabilizing nanocrystalline materials with dopants," *Acta Mater.*, vol. 55, no. 7, pp. 2329–2336, 2007.

[93] R. Birringer, "Nanocrystalline materials," *Mater. Sci. Eng. A*, vol. 117, no. C, pp. 33–43, 1989.

[94] J. Weissmüller, "Alloy effects in nanostructures," *Nanostructured Mater.*, vol. 3, no. 1–6, pp. 261–272, Jan. 1993.

[95] A. P. Sutton and R. W. Balluffi, "Interfaces in Crystalline Materials," p. xxvii-819, 1995.

[96] J. R. Trelewicz and C. A. Schuh, "Grain boundary segregation and thermodynamically stable binary nanocrystalline alloys," *Phys. Rev. B -*

Condens. Matter Mater. Phys., vol. 79, no. 9, pp. 1–13, 2009.

[97] K. A. Darling, "Thermal Stability of Nanocrystalline Microstructures," North Carolina State University, 2009.

[98] A. Endo, H. S. Chauhan, T. Egi, and Y. Shiohara, "Materials research," *J. Mater. Res*, vol. 13, no. 5, pp. 1186–1196, 1998.

[99] L. Lu, N. R. Tao, L. B. Wang, B. Z. Ding, and K. Lu, "Grain growth and strain release in nanocrystalline copper," *J. Appl. Phys.*, vol. 89, no. 11 I, pp. 6408–6414, 2001.

[100] C. E. Krill, H. Ehrhardt, and R. Birringer, "Thermodynamic stabilization of nanocrystallinity," *Zeitschrift fuer Met. Res. Adv. Tech.*, vol. 96, no. 10, pp. 1134–1141, 2005.

[101] F. Liu and R. Kirchheim, "Comparison between kinetic and thermodynamic effects on grain growth," *Thin Solid Films*, vol. 466, no. 1–2, pp. 108–113, 2004.

[102] A. Michels, C. E. Krill, H. Ehrhardt, R. Birringer, and D. T. Wu, "Modelling the influence of grain-size-dependent solute drag on the kinetics of grain growth in nanocrystalline materials," *Acta Mater.*, vol. 47, no. 7, pp. 2143–2152, 1999.

[103] K. Boylan, D. Ostrander, U. Erb, G. Palumbo, and K. T. Aust, "An in-situ tem study of the thermal stability of nanocrystalline NiP," *Scr. Metall. Mater.*, vol. 25, no. 12, pp. 2711–2716, 1991.

[104] H. Höfler and R. Averback, "Grain growth in nanocrystalline TiO2 and its relation to Vickers hardness and fracture toughness," *Scr. Metall. Mater.*, vol. 24, no. c, pp. 2401–2406, 1990.

[105] Z. Q. Gao and B. Fultz, “Inter-dependence of grain growth, Nb segregation, and chemical ordering in FeSiNb nanocrystals,” *Nanostructured Mater.*, vol. 4, no. 8, pp. 939–947, 1994.

[106] A. J. Detor and C. A. Schuh, “Grain boundary segregation, chemical ordering and stability of nanocrystalline alloys: Atomistic computer simulations in the Ni-W system,” *Acta Mater.*, vol. 55, no. 12, pp. 4221–4232, 2007.

[107] B. K. VanLeeuwen, K. A. Darling, C. C. Koch, R. O. Scattergood, and B. G. Butler, “Thermal stability of nanocrystalline Pd81Zr19,” *Acta Mater.*, vol. 58, no. 12, pp. 4292–4297, 2010.

[108] P. Knauth, A. Charaï, and P. Gas, “Grain growth of pure nickel and of a Ni-Si solid solution studied by differential scanning calorimetry on nanometer-sized crystals,” *Scr. Metall. Mater.*, vol. 28, no. 3, pp. 325–330, 1993.

[109] J. H. Driver, “Stability of nanostructured metals and alloys,” *Scr. Mater.*, vol. 51, no. 8 SPEC. ISS., pp. 819–823, 2004.

[110] X. Zhang, N. Q. Vo, P. Bellon, and R. S. Averback, “Microstructural stability of nanostructured Cu-Nb-W alloys during high-temperature annealing and irradiation,” *Acta Mater.*, vol. 59, no. 13, pp. 5332–5341, 2011.

[111] E. Botcharova, J. Freudenberger, and L. Schultz, “Mechanical alloying of copper with niobium and molybdenum,” *J. Mater. Sci.*, vol. 39, no. 16–17, pp. 5287–5290, 2004.

[112] F. J. Humphreys, M. Hatherly, F. J. Humphreys, and M. Hatherly, “Chapter 4 – The Structure and Energy of Grain Boundaries,” in *Recrystallization and Related Annealing Phenomena*, 2004, pp. 91–119.

[113] M. Saber, C. C. Koch, and R. O. Scattergood, “Thermodynamic Grain Size

Stabilization Models: An Overview," *Mater. Res. Lett.*, vol. 3831, no. January, pp. 37–41, 2015.

[114] J. Weissrmiller, "Alloy thermodynamics in nanostructures," *J. Mater. Res*, vol. 9, no. 1, pp. 21–24, 1994.

[115] J. Weissmüller, W. Krauss, T. Haubold, R. Birringer, and H. Gleiter, "Atomic structure and thermal stability of nanostructured Y-Fe alloys," *Nanostructured Mater.*, vol. 1, no. 6, pp. 439–447, 1992.

[116] R. Kirchheim, "Grain coarsening inhibited by solute segregation," *Acta Mater.*, vol. 50, no. 2, pp. 413–419, 2002.

[117] D. McLean, *Grain Boundaries in Metals Monographs on the Physics and Chemistry of Materials*. Clarendon Press, Oxford, 1957.

[118] R. Defay, I. Prigogine, A. A. Bellemans, and D. H. Everett, "Surface tension and adsorption," vol. 333, no. 1947, pp. 1947–1950, 1966.

[119] P. Wynblatt and R. C. Ku, "Surface energy and solute strain energy effects in surface segregation," *Surf. Sci.*, vol. 65, no. 2, pp. 511–531, 1977.

[120] P. Wynblatt and D. Chatain, "Anisotropy of segregation at grain boundaries and surfaces," *Metall. Mater. Trans. A*, vol. 37, no. 9, pp. 2595–2620, Sep. 2006.

[121] J. Friedel and J., "Electronic structure of primary solid solutions in metals," *Adv. Phys.*, vol. 3, no. 12, pp. 446–507, Oct. 1954.

[122] R. Kirchheim, "Reducing grain boundary, dislocation line and vacancy formation energies by solute segregation. I. Theoretical background," *Acta Mater.*, vol. 55, no. 15, pp. 5129–5138, 2007.

[123] R. Kirchheim, "Reducing grain boundary, dislocation line and vacancy

formation energies by solute segregationII. Experimental evidence and consequences," *Acta Mater.*, vol. 55, no. 15, pp. 5139–5148, 2007.

[124] P. C. Millett, R. P. Selvam, S. Bansal, and A. Saxena, "Atomistic simulation of grain boundary energetics - Effects of dopants," *Acta Mater.*, vol. 53, no. 13, pp. 3671–3678, 2005.

[125] F. Liu and R. Kirchheim, "Nano-scale grain growth inhibited by reducing grain boundary energy through solute segregation," *J. Cryst. Growth*, vol. 264, no. 1–3, pp. 385–391, 2004.

[126] A. J. Detor and C. A. Schuh, "Tailoring and patterning the grain size of nanocrystalline alloys," *Acta Mater.*, vol. 55, no. 1, pp. 371–379, 2007.

[127] T. Chookajorn, H. A. Murdoch, and C. A. Schuh, "Design of stable nanocrystalline alloys," *Science (80-.).*, vol. 337, no. 6097, pp. 951–4, 2012.

[128] B. D. Cullity, *Elements of X-ray diffraction*, 2nd ed. Addison-Wesley Publ. Co. Read. MA, 1978.

[129] H. K. and L. Alexander, *X-Ray Diffraction Procedures: For Polycrystalline and Amorphous Materials*. New York: John Wiley & Sons, 1974.

[130] B. D. Cullity and S. R. Stock, "Elements of X-ray diffraction, 3rd edition," *Prentice Hall*, p. Chapter 1, 2001.

[131] D. B. Williams and C. B. Carter, "The Transmission Electron Microscope," *Transm. Electron Microsc.*, pp. 3–17, 1996.

[132] R. F. Egerton, *Physical Principles of Electron Microscopy*, vol. 24, no. 5. 2005.

[133] "SPI Supplies Disc Punch, Produces 2 mm Discs : 17003-AB : SPI Supplies." [Online]. Available: http://www.2spi.com/item/17003-ab/grid-punch/. [Accessed: 10-Mar-2017].

[134] “Model 110 Automatic Twin-Jet Electropolisher.” [Online]. Available: http://www.fischione.com/products/conventional-specimen-preparation/model-110-automatic-twin-jet-electropolisher. [Accessed: 10-Mar-2017].

[135] D. V. S. Rao, K. Muraleedharan, and C. J. Humphreys, “TEM specimen preparation techniques,” *Microsc. Sci. Technol. Appl. Educ.*, no. 320, pp. 1232–1244, 2010.

[136] D. Tabor, “The Hardness of Metals,” *Nature*, vol. 170, no. 4333. pp. 818–818, 1952.

[137] I. M. Hutchings, “The contributions of David Tabor to the science of indentation hardness,” *J. Mater. Res.*, vol. 24, no. 3, pp. 581–589, 2009.

[138] American Society for Testing and Materials, “Standard Test Method for Knoop and Vickers Hardness of Materials,” *ASTM Stand. E384-11*, pp. 1–43, 2012.

[139] ASM International, “Introduction to Tensile Testing,” *Tensile Test.*, pp. 1–13, 2004.

[140] “Variable Pressure Scanning Electron Microscope – Hitachi S3200N | AIF - NC State University.” [Online]. Available: https://www.aif.ncsu.edu/equipment/variable-pressure-scanning-electron-microsocpe-vpsem/. [Accessed: 14-Apr-2017].

[141] F. M. Smits, “Measurement of Sheet Resistivities with the Four-Point Probe,” *Bell Syst. Tech. J.*, vol. 37, no. 3, pp. 711–718, 1958.

[142] M. Sain, S. Ummartyotin, J. Juntaro, C. Wu, and H. Manuspiya, “Deposition of PEDOT: PSS nanoparticles as a conductive microlayer anode in OLEDs device by desktop inkjet printer,” *J. Nanomater.*, 2011.

[143] H. Okamoto, “Cu-Nb (Copper-Niobium),” *J. Phase Equilibria*, vol. 12, no. 5,

pp. 614–615, 1991.

[144] L. He and E. Ma, “Processing and microhardness of bulk Cu-Fe nanocomposites,” *Nanostructured Mater.*, vol. 7, no. 3, pp. 327–339, 1996.